

1 **Investigation of organic matter and biomarkers from**
2 **Diepkloof Rock Shelter, South Africa: insights into Middle**
3 **Stone Age site usage and palaeoclimate**

4 James A. Collins^{1*}, Andrew S. Carr², Enno Schefuß³, Arnoud Boom², Judith Sealy⁴

5 1) Alfred Wegener Institute for Polar and Marine Research, Am Alten Hafen 26,
6 D-27568 Bremerhaven, Germany

7 2) Department of Geography, University of Leicester, University Road, Leicester
8 LE1 7RH, UK

9 3) MARUM – Center for Marine Environmental Sciences, University of Bremen,
10 Leobener Strasse 8, D-28359 Bremen, Germany

11 4) Department of Archaeology, University of Cape Town, Private Bag X3,
12 Rondebosch 7701 South Africa

13 * Now at: GFZ-German Research Centre for Geosciences, Section 5.1
14 Geomorphology, Telegrafenberg, Potsdam 14473, Germany

15 **Abstract**

16 Diepkloof Rock Shelter (DRS) represents a site of major interest for
17 reconstructing early human behaviours during the Middle Stone Age (MSA).
18 Rock shelters such as DRS also potentially preserve information concerning the
19 environmental context for such behaviours. In this respect the organic matter
20 composition of rock shelter sediments has rarely been investigated in detail,

21 particularly at the molecular level. Here, we used pyrolysis-gas
22 chromatography/mass spectrometry (py-GC/MS) to systematically assess the
23 organic matter composition of bulk sediments within the MSA and Later Stone
24 Age (LSA) sequence at DRS. From this we sought to gain insights into site usage,
25 taphonomy and burning practices. Additionally, we analyzed the chain length
26 distribution of leaf-wax *n*-alkanes as well as their hydrogen and carbon isotopic
27 compositions (δD_{wax} and $\delta^{13}C_{wax}$) to investigate their potential as hydroclimate
28 and vegetation indicators. This constitutes the first leaf-wax isotopic data in a
29 terrestrial context of this antiquity in South Africa.

30 Py-GC/MS shows a dichotomy between stratigraphic units (SUs) of high organic
31 matter content, producing a range of pyrolysis products, including homologous
32 series of long chain *n*-alkene/*n*-alkane doublets and alkyl-nitriles, and SUs of low
33 organic matter content, dominated by aromatic, heterocyclic N and polycyclic
34 aromatic hydrocarbon (PAH) pyrolysis products; typical molecular burning
35 products. Several SUs of the Intermediate Howiesons Poort interval exhibit the
36 latter composition, consistent with micromorphological evidence.

37 $\delta^{13}C_{wax}$ remains stable throughout the MSA, but leaf-wax *n*-alkane chain length
38 and δD_{wax} increase during the Late Howiesons Poort interval. Comparison with
39 such patterns in modern plants in the region suggests this represents a shift
40 towards the input of more arid-adapted vegetation into the shelter, driven either
41 by aridification at the site locale or a change in selection practices. Our results
42 suggest that these techniques have further potential in southern Africa and
43 globally at sites where organic matter preservation is high.

44 **Key words**

45 Organic matter composition, py-GC/MS, $\delta^{13}\text{C}_{\text{wax}}$, $\delta\text{D}_{\text{wax}}$, PAHs, *n*-alkane chain
46 length distribution, burning

47 **1. Introduction**

48 Diepkloof Rock Shelter (DRS), Western Cape Province, South Africa (**Fig. 1**) hosts
49 a sequence spanning the pre-Still Bay to Howiesons Poort industries of the
50 Middle Stone Age (MSA), and is overlain by Later Stone Age deposits (LSA;
51 Porraz et al., 2013; **Fig. 2a**). The site has yielded a multitude of findings,
52 including lithic artefacts (Porraz et al., 2013), charcoal remains (Cartwright,
53 2013; Miller et al., 2013), specific hafting residues (Charrié-Duhaut et al., 2013),
54 ochre (Dayet et al., 2013) and faunal remains (Steele and Klein, 2013). Perhaps
55 the most remarkable finding is the earliest evidence for engraved ostrich
56 eggshell (EOES) during the Early Howiesons Poort interval (Texier et al., 2013),
57 thought to represent a significant cultural and social development (Texier et al.,
58 2010). Developing an environmental context for such cultural/social
59 developments, both at DRS and beyond (e.g. Henshilwood et al., 2002) has,
60 however, proved challenging in this locale and on the wider southern Cape
61 (Chase, 2010), fundamentally reflecting the lack of contemporaneous terrestrial
62 environmental archives (Carr et al., 2016b).

63 Faunal remains and stone tool assemblages from MSA sites often provide
64 valuable archaeological and environmental insights. However, it has been noted
65 that there is often relatively limited consideration of the organic material within
66 many MSA deposits (Wadley, 2015). In cases where organic material has been
67 directly analysed, striking insights have been provided, including identification

68 of bedding structures (Goldberg et al., 2009; Wadley, 2011) and specific
69 geochemical evidence for the use of chemical adhesives (Charrié-Duhaut et al.,
70 2013). Here we consider the molecular character of sedimentary organic matter
71 in an archaeological context both to support archaeological inference and to gain
72 insights into environmental change. We specifically aim to investigate questions
73 surrounding the degree of burning, the types of vegetation brought into the site
74 and evidence for past hydroclimatic change. We characterize the organic
75 composition of the sediments and assess the degree to which each stratigraphic
76 unit was burnt using pyrolysis-gas chromatography/mass spectrometry (py-
77 GC/MS), while vegetation type and hydroclimate are considered via the
78 distribution and isotopic composition of leaf-wax *n*-alkanes.

79 **2. Diepkloof Rock Shelter background and setting**

80 **2.1 Setting and stratigraphy**

81 DRS is located at ~120m altitude above the Verlorenvlei wetland about 14km
82 from the modern coastline. The rock shelter formed within a quartzitic sandstone
83 butte, and has a floor area of 200m². Based on stone tool assemblages, the
84 sedimentary sequence within the shelter has been ascribed to different techno-
85 cultural phases of the MSA (Porraz et al., 2013). From bottom to top the complete
86 sequence includes the Lower MSA, MSA 'Mike', pre-Still Bay, Still Bay, Early
87 Howiesons Poort, MSA 'Jack', Intermediate and Late Howiesons Poort and finally
88 the post-Howiesons Poort (Porraz et al., 2013); here we focus on the pre-Still Bay
89 to Late Howiesons Poort (**Fig. 2**). The sequence has been further divided into
90 Stratigraphic Units (SUs), which represent complexes of individual lenses and
91 beds (microfacies; Miller et al., 2013), given names ordered mainly alphabetically
92 from the top to the base.

93 Micromorphological analysis indicates that the sediments in the rockshelter
94 comprise ash, charcoal and siliciclastic fragments, as well as bone, eggshell, and
95 humified organic remains (Miller et al., 2013). The upper part of the section,
96 corresponding to the Intermediate and Late Howiesons Poort, displays evidence
97 for the raking out of hearths and the burning of bedding, suggesting more
98 frequent or intensive site use (Miller et al., 2013).

99 In terms of palaeoclimate and palaeovegetation, charcoal remains indicate
100 variability in the vegetation brought to the shelter between the Still Bay and
101 Howiesons Poort (Cartwright, 2013). During the Still Bay, the charcoal
102 assemblage comprises a range of both Afromontane forest and thicket taxa, while
103 during the Howiesons Poort, vegetation indicates a wider range of taxa, including
104 more thicket and shrubland woody taxa, implying a shift towards more arid
105 conditions (Cartwright, 2013). Faunal remains have also yielded insights into the
106 past vegetation of the region. Evidence for grazers, rare during the LSA, was
107 taken to indicate that more grassy conditions prevailed during the MSA relative
108 to the LSA (Steele and Klein, 2013), although in this context the exposed
109 continental shelf, which was up to ~20km in extent during the period of MSA
110 occupation (Porraz et al., 2013), may account for some changes in faunal
111 assemblage.

112 Given that vegetation brought to the site was selected by the inhabitants and
113 represents only a specific fraction of the vegetation surrounding the site, it is also
114 plausible that the above changes in vegetation and faunal assemblage reflect
115 changes in selection practises by the inhabitants. Nonetheless, it may be argued
116 that on these long timescales, climate is the overarching control on the available

117 vegetation. Either way, this represents an important aspect to bear in mind when
118 interpreting our data.

119 **2.2 Chronology of the DRS sequence**

120 The LSA sequence at DRS is believed to span the last 1.8 ka (Parkington and
121 Poggenpoel, 1987). For the MSA sequence, two different optically stimulated
122 luminescence (OSL) chronologies have been proposed. The initial chronology
123 from grid squares C6 and L6 within the shelter (Jacobs and Roberts, 2015; Jacobs
124 et al., 2008) indicated that the Still Bay to Late Howiesons Poort industries span
125 an age range of 73.6 ± 2.5 ka to 60.5 ± 1.9 ka. Later studies using both
126 thermoluminescence and single grain OSL (Feathers, 2015; Tribolo et al., 2013;
127 Tribolo et al., 2009) from grid squares M7, N7, L6 and M6 and P11-Q11 (for OB2-
128 4) suggest that the Still Bay to Late Howiesons Poort spans an age range between
129 109 ± 10 ka to 52 ± 5 ka and tend to be clustered, with the Still Bay (109 ± 10 ka)
130 producing a similar age to the Early Howiesons Poort (105 ± 10 ka to 109 ± 10
131 ka) and the Intermediate Howiesons Poort dated at 85 ± 9 ka to 77 ± 8 ka. The
132 late Howiesons Poort is much younger (52 ± 5 ka), although this is taken from
133 the back sector of the excavation (Tribolo et al., 2013). The disparities in these
134 chronologies are yet to be resolved (Jacobs and Roberts 2015, Feathers 2015). As
135 some dated samples were obtained from different grid squares of the site these
136 differences may reflect some as yet undiscerned stratigraphic complexity at the
137 site. As such, because our samples were taken closest to material analysed by
138 Tribolo et al., (2013), we refer to their ages.

139 2.3 Climate and vegetation of the region

140 The locale around DRS comprises a mosaic of vegetation (Cartwright 2013).
141 Briefly, steep rocky kloofs (ravines) provide shelter and retain enough soil
142 moisture to permit growth of some occasional trees and mesic thicket taxa
143 including small trees and shrubs. Going downslope from the shelter, crevices and
144 large boulders retain enough moisture to permit growth of thicket, while further
145 downslope, sandy soils favour the growth of asteraceous shrubs, seasonal bulbs,
146 succulents and grasses.

147 DRS is positioned within the Lowland Fynbos biome, just south of the boundary
148 with the Succulent Karoo biome (**Fig. 1a**). The Fynbos biome (comprising the
149 Lowland and Montane Fynbos eco-regions), which extends to the southwest of
150 DRS is a Mediterranean-type shrubland comprising sclerophyllous proteoid
151 shrubs, small-leaved ericoid shrubs (notably from the Ericaceae family), Cape
152 reeds (Restionaceae) and various geophytes from the Liliaceae and Iridaceae
153 families (Cowling et al., 1997). The vegetation of the Fynbos biome is
154 characterised by a general absence of trees and adaptation to summer drought.
155 There are a small number of CAM species, but most plants use the C₃ pathway
156 (Vogel et al., 1978). Some halophytic C₄ vegetation occurs on the banks of the
157 Verlorenvlei wetland (Carr et al., 2015). DRS receives ~250 mm of precipitation
158 per year, which is delivered mostly (70%) during austral winter. Regions south
159 and west of DRS are less arid (**Fig. 1b**) and receive 200-500 mm of precipitation
160 per year, delivered mainly (70-90%) during winter.

161 The Succulent Karoo biome (**Fig. 1a**) to the north of DRS is characterised by a
162 generally hotter and more arid climate (**Fig. 1b**), particularly during the summer,

163 and the biome comprises more drought-adapted species such as leaf succulents
164 and dwarf shrubs from the Aizoaceae, Crassulaceae and Euphorbiaceae families
165 (Milton et al., 1997). Many species in the Succulent Karoo use CAM
166 photosynthesis (Rundel et al., 1999) and are characterised by thick, waxy
167 cuticles, dwarf succulence and shallow rooting systems. In the northern
168 Succulent Karoo, mean annual rainfall is approximately 150-300 mm yr⁻¹
169 (Hijmans et al., 2005), and seasonality is markedly reduced (~50% during the
170 winter).

171 **3. Background to the organic matter and molecular approach**

172 **3.1 Rockshelter organic matter composition**

173 Micromorphological analyses suggest terrestrial plants represent a significant
174 component of the organic material preserved in rockshelter sediments (Miller et
175 al. 2013), along with burning products, be they derived originally from plants
176 (Cartwright, 2013) or animal products (Goldberg et al., 2009; Miller et al., 2013).
177 The major organic components of fresh vegetation include macromolecular
178 lignin, cellulose and leaf cuticles (e.g. cutin macromolecule); the latter is also
179 associated with the synthesis of soluble leaf waxes. While cellulose has a low
180 preservation potential in the arid environments of southern Africa (Carr et al.,
181 2010; 2013), sedimentary lignin monomers can be used to reconstruct past
182 vegetation types (Goñi and Hedges, 1992), although their preservation can be
183 variable (Thevenot et al., 2010). Leaf-wax lipids, particularly *n*-alkanes, tend to
184 be relatively well preserved in a variety of sedimentary contexts and are
185 preserved within soils throughout the study area (Carr et al., 2014).

186

187 Incomplete or variable combustion of organic matter, as would be anticipated in
188 an archaeological context, generates a continuum of organic materials (Masiello,
189 2004), with more prolonged burning or higher temperatures producing organic
190 matter increasingly dominated by PAHs, and other aromatic compounds
191 characterised by the presence of more ring structures (e.g. Simoneit, 2002).

192 To assess the organic matter composition of DRS sediments we use py-GC/MS,
193 which can be performed directly on sediments, without extraction. Pyrolysis
194 thermally fragments macromolecules in an inert atmosphere, rendering large
195 macromolecular compounds (such as cellulose and lignin) amenable to GC
196 analysis (e.g. Sáiz-Jiménez and De Leeuw, 1986). Our aims are to compare the
197 organic matter components preserved in the MSA (late Pleistocene) and LSA
198 (late Holocene) sediments and to identify whether burning indicators (e.g. PAHs)
199 relative to unburnt compounds (e.g. leaf waxes) change through the sequence
200 and how this relates to other cultural/societal changes.

201 **3.2 Leaf-wax *n*-alkanes**

202 We also analysed leaf-wax *n*-alkanes, which are commonly utilized in
203 palaeoenvironmental research, given their suitability for compound-specific
204 hydrogen and carbon isotopic analysis (Eglinton and Eglinton, 2008). Leaf-wax
205 derived *n*-alkanes are typically long-chain compounds, with a chain length
206 distribution between about 25 and 33 carbon atoms (C₂₅-C₃₃) and a strong
207 tendency for odd/even chain length preference (Eglinton and Hamilton, 1967).

208 The chain-length distribution of leaf-wax *n*-alkanes can provide information
209 regarding vegetation type (e.g. Poynter et al., 1989; Vogts et al., 2009). In the
210 Western Cape, the *n*-alkane distributions from the Fynbos biome are, on average,

211 distinct from those of the Succulent Karoo (Carr et al., 2014). Fynbos vegetation
212 tends to be C₃₁ and C₂₉ dominated while Succulent Karoo vegetation tends to be
213 dominated by *n*-alkanes of C₃₁ and C₃₃ chain length (**Fig. 3a**), which likely reflects
214 the combined effects of a more arid climate and the associated transition to more
215 drought-adapted plants within the Succulent Karoo biome. This feature of the
216 chain length distribution is typically summarized (Carr et al., 2014; Schefuß et al.,
217 2003) using the Norm31 index (C₃₁/C₃₁+C₂₉). Vegetation of the Lowland Fynbos
218 biome is thus characterized by lower Norm31 values (mean of 0.57 ± 0.31, n=28)
219 than the Succulent Karoo (mean of 0.84 ± 0.17; n=133; **Fig. 1a**; Carr et al., 2014;
220 Herrmann et al., 2016).

221 Compared to soils and sedimentary environments, there are additional factors
222 affecting leaf-wax preservation within an archaeological site. Laboratory and
223 field burning experiments show that incomplete combustion of leaf waxes
224 increases the proportion of shorter chain length and even-numbered *n*-alkanes
225 due to fragmentation of the longer homologues, with greater fragmentation
226 occurring with higher combustion temperatures (Eckmeier and Wiesenberg,
227 2009; Mallol et al., 2013; Wiesenberg et al., 2009). The *n*-alkane average chain
228 length (ACL₁₄₋₃₅) of maize straw dropped from 30.2 to 25.8 when burnt at 300°C
229 and to 17.4 at 500°C (Wiesenberg et al., 2009). The odd-over-even number
230 preference of the waxes, summarised by the carbon preference index (CPI₂₇₋₃₃,
231 where values around 1 indicate no odd-over-even preference), was reduced from
232 10.7 when unburnt, to 2.6 at 300°C and then 0.9 at 500°C (Eckmeier and
233 Wiesenberg, 2009; Wiesenberg et al., 2009).

234 We aim to determine to what degree the leaf-wax chain-length distribution of
235 DRS sediments reflects the primary vegetation versus combustion processes and
236 whether the Norm31 index can elucidate past changes in vegetation input.

237 **3.3 Leaf-wax isotopes (δD_{wax} and $\delta^{13}C_{wax}$)**

238 δD_{wax} is commonly utilized as a palaeohydrological indicator. Precipitation is the
239 ultimate source of hydrogen for leaf waxes and δD_{wax} typically records changes
240 in precipitation δD (δD_p ; Sachse et al., 2012), which in turn reflects precipitation
241 source and/or amount (Rozanski et al., 1993). Relative humidity and plant type
242 exert secondary effects on δD_{wax} (Sachse et al., 2012).

243 The potential of δD_{wax} analysis in the Western Cape was demonstrated by
244 Herrmann et al., (2017), who showed reasonably coherent changes in δD_{wax} with
245 aridity for contemporary soils from across the sub-continent (**Fig. 1b**). Higher
246 δD_{wax} in the Succulent Karoo biome likely reflects lower precipitation amounts
247 and increased evapotranspiration associated with long dry summers. The
248 Western Cape (broadly, winter rainfall zone), however, displays a complicated
249 spatial pattern, possibly due to the effects of both summer and winter rainfall,
250 the existence of microclimates and a diverse array of vegetation types in this
251 mountainous region (Herrmann et al., 2017).

252 $\delta^{13}C_{wax}$ is a function of photosynthetic pathway and aridity, and is commonly
253 interpreted as a palaeovegetation indicator. C_3 plants from the Succulent Karoo
254 exhibit mean $\delta^{13}C_{wax}$ values of $-34.2\text{‰} \pm 4\text{‰}$ for the C_{31} *n*-alkane (Boom et al.,
255 2014). CAM plants from the Succulent Karoo display higher but also more
256 variable values (a mean C_{31} *n*-alkane $\delta^{13}C_{wax}$ value of $-22.7\text{‰} \pm 6\text{‰}$), with

257 facultative CAM plants displaying a mean of $-28.9\text{‰} \pm 3\text{‰}$ (Boom et al., 2014).
258 C_4 grasses exhibit an average C_{31} *n*-alkane $\delta^{13}C_{\text{wax}}$ value of $-21.8\text{‰} \pm 2\text{‰}$
259 (Rommerskirchen et al., 2006). The transect of southern African soils (Herrmann
260 et al., 2016) displays an increase in $\delta^{13}C_{\text{wax}}$ in the Succulent Karoo to the NE of
261 the study site.

262 The effect of burning or heating of *n*-alkanes might potentially affect δD_{wax} and
263 $\delta^{13}C_{\text{wax}}$ values. Bulk plant $\delta^{13}C$ values display isotopic enrichment ($\sim 1\text{‰}$) after
264 burning (Poole et al., 2002), related to preferential loss of isotopically light
265 components. Previous compound-specific work on this topic is, however, limited,
266 although it has been shown that mid-chain length fatty acids from aerosols
267 produced during burning exhibit both increased and decreased $\delta^{13}C$ values,
268 depending on the plant type (Ballentine et al., 1998), and thus reveal no
269 systematic effect. It is thought that the mid-chain length compounds formed from
270 chemical degradation during burning and the isotopic composition of the
271 precursor molecules varies between plant types. This process is, however,
272 unlikely to apply to long-chain leaf waxes such as the C_{31} *n*-alkane, which likely
273 represent the intact original compounds.

274 At DRS we aim to investigate whether the leaf-wax isotopic composition reflects
275 the primary vegetation and hydroclimate signals or has been overprinted by
276 burning processes. Moreover, we aim to elucidate how vegetation, hydroclimate
277 and/or human selection practices have changed over time.

278 4. Methods

279 4.1 Sampling

280 Sediment samples were collected during the field season of 2013. Samples were
281 taken from the standing section. Sediment on the exposed surface was scraped
282 away, and the immediately underlying sediment scraped into glass vials using a
283 metal spoon that was wiped clean between samples. Samples from the MSA
284 levels were taken in grid square M7B, adjacent to the location of samples for
285 micromorphological analysis reported by Miller et al., (2013). Thirty-one
286 samples were taken in total, spanning SUs Lynn to Debbie (**Fig. 2**). This includes
287 two samples from each of SUs Eve, Frans and Leo to assess the variability within
288 individual SUs. LSA deposits were not preserved in this area of the site, so three
289 LSA samples were taken where deposits of this age were exposed. LSA 1 came
290 from the C6/C7 profile. LSA 2 was taken from the M5/M4 profile, in
291 approximately the middle of the square. LSA 3 came from the E6/E5 profile. Most
292 of the LSA deposits at Diepkloof occur as pits dug into the MSA layers. While
293 every effort was made to ensure that the LSA samples consisted of pit infill, it is
294 impossible to be certain that there is no admixture of MSA sediments.

295 4.2 Bulk parameters (%TC, bulk $\delta^{13}\text{C}_{\text{TC}}$, %TN and bulk $\delta^{15}\text{N}$)

296 In addition to the molecular indicators, we also analyzed bulk parameters. Bulk
297 measurements of total carbon (%TC; including black carbon and organic
298 carbon), bulk $\delta^{13}\text{C}_{\text{TC}}$, total nitrogen (%TN) and bulk $\delta^{15}\text{N}$ were determined at the
299 University of Cape Town, after pre-treatment with 1M hydrochloric acid to
300 remove carbonates. Samples were combusted at 1020°C in a Flash 2000
301 elemental analyser and the resultant gases analysed with a Delta V Plus isotope

302 ratio mass spectrometer (ThermoScientific, Germany). Duplicate analyses of
303 homogeneous material yielded a typical precision of 0.2‰ for both carbon and
304 nitrogen isotopic measurements.

305 4.3 Pyrolysis-Gas Chromatography/Mass Spectrometry (py-GC/MS)

306 For py-GC/MS we analysed a subset of twenty MSA samples and all three LSA
307 samples. Py-GC/MS was performed using a CDS1000 pyroprobe interfaced with
308 a Perkin Elmer Clarus 500 GC/MS system. 25-50 mg of dried sediment (not
309 previously solvent extracted) was encapsulated in a quartz tube, rested in the
310 pyrolysis interface (at 300°C for 3 min) to minimise the inclusion of evaporated
311 compounds (Sáiz-Jiménez, 1994), and then pyrolysed at 610 °C for 15 s. Gas
312 chromatography was carried out using a CP-Sil 5CB MS column (30 m × 0.25 mm
313 × 0.32 µm). The GC temperature programme began at 40 °C (1.8 min), was
314 ramped to a final temperature of 310 °C at 4 °C min⁻¹ and held for a further 20
315 min. Compounds within the pyrograms were identified based on their mass
316 spectra and retention times (e.g. **Fig. 5**). Peak integrations were performed using
317 the Turbo-Mass 5.2.0 software.

318 The relative proportion of each compound was determined using the summed
319 integrations for all identified compounds (up to a total of 148) in each pyrogram
320 (e.g. Carr et al., 2010b; Vancampenhout et al., 2008). Each compound was
321 classified into one of eight categories (e.g. Kaal et al., 2007) comprising: 1)
322 aliphatics (*n*-alkanes, *n*-alkenes, fatty acids); 2) nitrogen-containing compounds,
323 dominated by alkyl nitriles, but also associated with 3) some heterocyclic
324 aromatic moieties, such as (*n*-methyl) pyrrole, pyridine, and quinoline; 4)
325 aromatics (e.g. benzene, xylene and alkylbenzenes); 5) polycyclic aromatic

326 hydrocarbons (PAHs; (*n*-methyl) naphthalene, biphenyl, (*n*-methyl) fluorene,
327 anthracene); 6) lignin pyrolysis products (known products of coniferyl, syringyl,
328 and coumaryl moieties); 7) phenolic compounds (e.g. phenol and methyl
329 phenols); 8) polysaccharide products (primarily furans and levoglucosan).

330 To provide further insight into the most probable macromolecular structures
331 and precursor compounds, pyrolysis was performed on three samples (LSA 1,
332 Logan and Ester) in the presence of tetramethylammonium hydroxide (TMAH)
333 (Challinor, 2001; Del Rio and Hatcher, 1998). This procedure, known as
334 thermally assisted hydrolysis and methylation, limits the degree of
335 fragmentation during pyrolysis and is also capable of transmethylation of ester
336 bonds; hence it depolymerizes important biopolyesters such as cutin.

337 **4.4 Leaf-wax extraction, purification and quantification**

338 For leaf wax analysis, we extracted all thirty-one MSA samples. 2.6g to 5.8g of
339 dried sediment were extracted using an DIONEX ASE350 accelerated solvent
340 extractor at 100°C using a solvent mix of DCM:MeOH (2:1) for 5 minutes
341 repeated 3 times. The apolar fraction containing *n*-alkanes was obtained by
342 elution of the dried lipid extract with hexane over a silica gel column (mesh size
343 60) followed by subsequent elution with hexane over AgNO₃ to remove
344 unsaturated compounds.

345 *n*-Alkanes were identified using GC-FID, by comparison of retention times with
346 an external standard mix. Squalane internal standard added before extraction
347 yielded variable extraction recoveries, likely due to adsorption onto the complex
348 organic matrix. We quantified *n*-alkane amounts by comparison with an external
349 standard. Based on repeated analyses of an external alkane standard the

350 quantification precision is <5%. We characterised the *n*-alkane distribution using
351 standard parameters CPI₂₅₋₃₃, ACL₁₄₋₃₅ and Norm31 (following e.g. Carr et al.,
352 2014, and references therein).

353 4.5 Leaf-wax isotopic analyses

354 $\delta^{13}\text{C}_{\text{wax}}$ was analysed using a ThermoFischer Scientific Trace Gas Chromatograph
355 coupled to a Finnigan MAT 252 isotope ratio monitoring mass spectrometer (GC-
356 IRMS) via a combustion interface operated at 1000°C. Isotope values were
357 calibrated against external CO₂ reference gas and are reported in ‰ relative to
358 VPDB. Samples were run in duplicate, with an average reproducibility of 0.1‰
359 for the C₃₁ *n*-alkane. Leaf-wax *n*-alkane $\delta\text{D}_{\text{wax}}$ was measured using a
360 ThermoFisher Scientific Trace GC coupled, via a pyrolysis reactor operated at
361 1420°C, to a ThermoFisher MAT 253 isotope ratio mass spectrometer. δD values
362 were calibrated against external H₂ reference gas and are reported in ‰ relative
363 to VSMOW. Samples were analysed in duplicate with an average reproducibility
364 of 1‰ for the C₃₁ *n*-alkane. Repeated analysis of an external *n*-alkane standard
365 between samples yielded a root-mean-squared accuracy of 2‰ and a standard
366 deviation of on average 3‰. The H₃-factor, used to correct for the formation of
367 H₃⁺ in the ion source, had a mean of 6.0 and varied between 5.8 and 6.2
368 throughout the analyses. Isotopic measurements were not made on samples
369 Fran, Base of Frans, Fred, Frank, Fox, Fiona, Governor, Jack, Jude, Julia, Kate, Leo2
370 and Lynn due to low leaf-wax content.

371 5. Results

372 5.1 Bulk parameters

373 %TC is highly variable throughout the DRS sequence, ranging from ~2% to 37%
374 (**Fig. 4a**). Major spikes in %TC are seen in SUs Base of Frans, Fox, Fiona and
375 Kenny. The high values of the bulk %TC are likely attributable to high contents of
376 black carbon in the sediments, derived from combustion (Braadbaart et al., 2004;
377 Braadbaart and Poole, 2008). However, %TC also incorporates organic carbon,
378 which complicates the interpretation of %TC, but may explain its high variability.
379 Bulk $\delta^{13}\text{C}_{\text{TC}}$ displays relatively little change, but tends to be lower during the SUs
380 of the Late Howiesons Poort, averaging -24‰, compared to the SUs of the Early
381 Howiesons Poort, which average -23‰ (**Fig. 4b**). %TN is high (up to 5%) and
382 co-varies with %TC (**Fig. 4c**). Bulk $\delta^{15}\text{N}$ is very high, with values of > 20‰
383 throughout much of the record (**Fig. 4d**). Bulk $\delta^{15}\text{N}$ values are highest, but also
384 most variable during the Late Howiesons Poort.

385 5.2 py-GC/MS

386 5.2.1 py-GC/MS in the absence of TMAH

387 The relative proportion of aliphatic compounds in the DRS sequence varies
388 between 0 to 69% of the integrated ion current. The main contributors to this
389 class are homologous sequences of *n*-alkane/*n*-alkene doublets spanning the
390 chain length range C₈-C₃₃ (**Fig. 5a,b**) Aliphatics are most prominent in samples
391 LSA 1-3, and SUs Lynn, Logan, Keeno, Kerry, Joy, Jeff, John, Base of Eve, Ester and
392 Eric (**Fig. 6**). The aliphatics include a high proportion of longer chain length *n*-
393 alkanes, with an odd-over-even preference (**Fig. 5a,b**), which are most likely

394 leaf-waxes that were not evaporated in the pyrolysis unit prior to analysis or
395 bound to the sediment.

396 A distinct feature of several DRS pyrolysates (e.g. SUs Kim, Julia, Jack, Frank, Fred
397 and Frans) is the presence of homologous sequences of alkyl-nitriles (up to C₂₂
398 and peaking at C₁₇ and C₁₅ in most cases (**Fig. 5a,b**), with the exception of Leo 1),
399 which make up 0-29% of the integrated ion current and are also of highest
400 abundance in LSA 1-3, and SUs Lynn, Logan, Keeno, Kerry, Joy, Jeff, John, Base of
401 Eve, Ester and Eric (**Fig. 6**).

402 Other nitrogen-containing compounds (i.e. excluding the alkyl-nitriles) include
403 heterocyclic aromatic compounds, (methyl) pyrrole, acetonitrile, (methyl)
404 pyridine, (methyl) indole, quinoline and (n-methyl) benzamide (**Fig. 5c**). The
405 heterocyclic N-compounds are not typically diagnostic of particular source
406 compounds but may be related to burning (Kaal and Rumpel, 2009). They make
407 up 4-80% of the integrated ion current and are most abundant in Leo2, Leo1,
408 Kim, Julia, Jack, Governor, Fiona, Frank, Fred, Base of Frans, Frans and Eve (**Fig**
409 **6**).

410 Aromatic compounds contribute 10 to 48% of the total ion current (**Fig. 6**). They
411 are dominated by benzene and to a lesser extent toluene and styrene (**Fig. 5c**).
412 Typically they are not diagnostic of particular source compounds, although have
413 been observed to increase in pyrolysates of materials associated with high
414 charring temperatures (Kaal et al., 2009; Kaal and Rumpel, 2009; Kaal et al.,
415 2012).

416 PAHs comprise up to 11% of the total ion current. Their abundance is
417 particularly high in SUs Governor, Fiona, Frank, Fred, and Base of Frans (**Fig. 6**).
418 The main contributors are naphthalene and small amounts of biphenyl, fluorene-
419 9-one, n-methyl naphthalenes and anthracene (**Fig. 5c**).

420 Lignin monomers are found only in the LSA samples, contributing 9-17% of the
421 total ion current. They are particularly well-preserved within LSA 1 (**Fig. 6**),
422 where we observe an extensive array of products from coniferyl and syringyl
423 lignin structures. Their absence in the MSA is likely due to degradation (Goñi and
424 Hedges, 1992). Phenolic compounds are only present in a few samples,
425 contribute up to 12% and are dominated by phenol. Their presence in the LSA
426 samples may partly reflect their derivation from lignin monomers (Vane and
427 Abbot 1999), or possibly proteins and tannins. Polysaccharides are present (2%-
428 5%) only in the LSA and are absent in the MSA.

429 **5.2.2 py-GC/MS in the presence of TMAH**

430 The three samples analysed in the presence of TMAH (LSA 1, Logan and Ester)
431 are dominated by C₁₄-C₂₀ Fatty Acid Methyl Esters (FAMES), peaking at C₁₆ and
432 C₁₈, with subordinate but variable contributions from long chain (C₂₄-C₃₂) FAMES
433 (**Fig. 5d-f**). The FAMES are most likely derived from bound carboxylic (fatty) acid
434 moieties and thus potentially a major source of the homologous alkane/alkene
435 doublets in the non-treated pyrolysates. The FAMES may, however, also be partly
436 derived from polymers, such as cutin (Del Rio and Hatcher 1998). The
437 homologous alkyl nitriles are present but much less abundant in the TMAH
438 analyses (**Fig. 5d-f**).

439 LSA 1 (**Fig. 5d**) produced multiple methylated lignin-related structures (e.g. the
440 methyl ester of 3,4,5 trimethoxy benzoic acid (syringyl derivative), *m*-anisic acid
441 methyl ester (4-methoxy benzoic acid methyl ester; *p*-coumaryl derivative) and
442 4-methy veratrole (3,4 dimethoxy toluene; guaiacyl derivative) consistent with
443 the untreated analyses. The 3,4,5 methyl ester of trimethoxy benzoic acid may,
444 however, also be tannin derived. Other features are the presence of *n*-methyl
445 benzamide, hippuric acid methyl ester, tetramethyl uric acid (1,3,7,9-
446 Tetramethyluric acid), and caffeine (1,3,7-Trimethylpurine-2,6-dione; structure
447 strongly related to tetramethyl uric acid). These compounds are atypical of
448 soils/Quaternary sediments within the study region (Carr et al 2014;
449 unpublished data) and in the case of the hippuric acid methyl ester have only
450 previously been reported, to our knowledge, in the pyrolysates of both rock
451 hyrax midden material (Carr et al., 2010a) and amberrat, the resinous excretion
452 of packrat urine (Fezzy and Armitage, 2006). Hippuric acid is a known
453 component of mammal urine (Bristow et al., 1992). Similarly, uric acid may be
454 derived from bird guano (Bird et al., 2008).

455 **5.3 Leaf-wax content and distribution**

456 For the solvent-extracted leaf waxes, contents are highly variable; they exhibit a
457 maximum of 18.2 $\mu\text{g g}^{-1}$ dw (for the C_{31} *n*-alkane; **Fig. 7**) but are below the
458 detection limit in SUs Jack, Governor, Fiona, Fox, Fred and Frans.

459 Leaf-wax CPI_{25-33} ranges between 1.9 and 16.3 (average = 9.6; **Fig. 8**). Leaf-wax
460 ACL_{14-35} ranges between 25.7 and 31.0 (average = 29.4) (**Fig. 8**). Through the
461 MSA, the ACL and CPI values display little overall trend, but SUs Leo2 and Debbie

462 display relatively low CPI, while SUs Leo2, Kate, Frank and Debbie display
463 relatively low ACL (**Fig. 8**).

464 The leaf-wax distribution of several SUs (e.g. Keeno) closely resembles the
465 average of modern Lowland Fynbos vegetation while other SUs (e.g. Eric)
466 resemble the average distribution of modern Succulent Karoo vegetation (**Fig.**
467 **3b**; Carr et al., 2014). For LSA 1- 3, Norm31 values range between 0.51 and 0.65
468 (**Fig. 9b**) and for the MSA values range between 0.54 and 0.83. For the SUs of the
469 Still Bay to Intermediate Howiesons Poort, values averaged 0.61 ± 0.05 , while for
470 SUs of the Late Howiesons Poort values increase to, on average, 0.74 ± 0.05 (**Fig.**
471 **9b**).

472 **5.4 Leaf-wax isotopes**

473 For samples LSA 1-3, $\delta^{13}\text{C}_{\text{wax}}$ for the C_{31} *n*-alkane (the most abundant and most
474 precisely measured homologue) ranges between $-29.7\text{‰} \pm 0.2\text{‰}$ and $-30.4\text{‰} \pm$
475 0.2‰ . and (**Fig. 9a**). For the SUs of the MSA, values exhibit a relatively small
476 range between $-29.9\text{‰} \pm 0.1\text{‰}$ and $-31.8\text{‰} \pm 0.1\text{‰}$. They are lowest in SUs Eve
477 and Base of Eve ($-31.8\text{‰} \pm 0.1\text{‰}$), during the Late Howiesons Poort.

478 For samples LSA 1-3, $\delta\text{D}_{\text{wax}}$ (**Fig. 9c**) ranges between $-130\text{‰} \pm 1\text{‰}$ and -147‰
479 $\pm 1\text{‰}$. Through the MSA, $\delta\text{D}_{\text{wax}}$ ranges between $-140\text{‰} \pm 1\text{‰}$ and $-116\text{‰} \pm$
480 1‰ . Values are generally lower (mean = $-133\text{‰} \pm 4\text{‰}$) for the SUs of the Still
481 Bay to Intermediate Howiesons Poort and higher (mean = $-120\text{‰} \pm 4\text{‰}$) for SUs
482 of the Late Howiesons Poort.

483 6. Discussion

484 6.1 py-GC/MS: organic matter composition

485 py-GC/MS shows a clear organic matter compositional dichotomy. LSA 1-3, and
486 SUs Lynn, Logan, Keeno, Kerry, Joy, Jeff, John, Base of Eve, Ester and Eric are rich
487 in organic material and yield a range of pyrolysis products, most notably
488 homologous sequences of *n*-alkane/*n*-alkene doublets and alkyl nitriles (**Fig.**
489 **5a,b**). Other samples (Leo2, Leo1, Kim, Julia, Jack, Governor, Fiona, Frank, Fred,
490 Base of Frans, Frans and Eve) yield fewer pyrolysis products, and are dominated
491 by aromatics and heterocyclic N (**Fig. 5c**). This major difference is inferred to
492 reflect samples relatively rich in less-altered plant material, versus those that
493 have undergone extensive burning or degradation.

494 Typical examples of SUs with a richer organic matter composition are John and
495 Jeff, which exhibit the highest relative proportion of homologous alkane/alkene
496 (aliphatic) pyrolysis products (**Fig. 6**). These are interpreted to be derived from
497 leaf cuticles, as revealed by the high abundance of long-chain FAMES produced
498 when the same samples are treated with TMAH (**Fig. 5d-f**), suggesting the
499 presence of relatively fresh, unburnt plant derived organic matter (although note
500 that more labile plant-derived OM such as lignin is not preserved in MSA SUs).

501 SUs exhibiting more burning include Leo 2, Kim, Julia, Jack, Governor, Fiona,
502 Frank, Fred, Base of Frans, Frans and Eve (**Fig. 6**). These produce far higher
503 proportions of aromatic, heterocyclic N, and PAH pyrolysis products, with low
504 abundances of aliphatics and leaf waxes. PAHs are particularly high for SUs
505 Governor to Base of Frans (**Fig. 6**), and these likely reflect the most intensely

506 heated samples (Kaal and Rumpel, 2009; Kaal et al., 2012). The pyrolysates show
507 some commonalities with black carbon pyrolysates (Kaal et al., 2008), but are
508 less diverse than pyrolysates of modern burned material (Kaal et al. 2009), likely
509 due to degradation within the more ancient MSA sediments. Based on laboratory
510 burning experiments, a number of ratios (benzene/toluene, naphthalene/C₁-
511 naphthalene) have been proposed as indicators of burning intensity (Kaal and
512 Rumpel, 2009; Kaal et al., 2012). The absence of toluene and C₁-naphthalene in
513 several SUs is likely due to incomplete preservation of these compounds.
514 Nonetheless, several PAH, aromatic and heterocyclic-N pyrolysis products (Kaal
515 and Rumpel 2009), are seen in the DRS pyrolysates (benzene, toluene,
516 naphthalene, biphenyl, dibenzofuran and benzonitrile) and we take the summed
517 integration of these as a summary indicator of black carbon and burning (**Fig.**
518 **10a**).

519 Although we often observe similarities in organic matter composition between
520 adjacent SUs, we also note differences within individual SUs. For example, Eve
521 and Base of Eve, and Leo 1 and Leo 2 display a different organic matter
522 composition (**Fig. 6**). This highlights large differences in composition between
523 individual depositional units (microfacies units) within each SU (Miller et al.,
524 2013).

525 Another point of note is that LSA 2 is compositionally anomalous compared to
526 LSA 1 and LSA 3 in terms of the py-GC/MS analyses (**Fig. 6**), leaf-wax distribution
527 and isotopic analyses (**Fig. 9**). This might reflect some admixing of the MSA
528 material into the LSA, which would account for the absence of lignin and

529 cellulose pyrolysis products in LSA 2, despite their conspicuous presence in LSA
530 1 and LSA 3.

531 **6.2 Nitrogen containing compounds**

532 Notable in the py-GC/MS data are the relatively high abundances of the nitrogen-
533 containing compounds in some samples, notably the homologous sequences of
534 alkyl nitriles. These are not observed in natural soils in the region, and the TN
535 content of the DRS sediments (**Fig. 4c**), is also substantially higher than modern
536 soils (Carr et al., 2013). Alkyl nitriles as pyrolysis products were previously
537 observed to form from the fragmentation of aliphatic molecules (probably the
538 C₁₈ fatty acid; **Fig 5e,f**) during pyrolysis in the presence of ammonia and clay
539 (Nierop and van Bergen, 2002). The source of ammonia at DRS may be related to
540 the hippuric acid and uric acid pyrolysis products identified in the LSA py-GC/MS
541 data. The latter is known to degrade to ammonia, explaining its absence in the
542 MSA pyrolysates (Mizutani and Wada, 1985), while micromorphological analyses
543 have previously identified a thick niter crust at the top of the sediments (Miller
544 et al., 2013). Rock hyraxes were identified as a likely N source in the sediments
545 (Miller et al., 2013) and the presence of benzamide, uric acid/hippuric acid
546 (methylated forms) in the LSA pyrolysates is consistent with the composition of
547 hyraceum, strongly pointing to urine contributions in two of the LSA samples
548 (Carr et al., 2010a; Fezzy and Armitage, 2006). Guano, however, might be an
549 additional source of N (Miller et al., 2013) and of the very high bulk $\delta^{15}\text{N}$ values
550 of the DRS sediment (19-32‰; **Fig. 4d**), which are significantly higher than local
551 vegetation (typically -4 to 5‰ (Sealy et al., 1987; Stock et al., 1995), soils
552 (typically 7-10‰ in the Lowland Fynbos; Carr et al., unpublished data), and

553 hyraceum (typically 5-10‰; (Carr et al., 2016a)). The impact of guano on soil
554 $\delta^{15}\text{N}$ has been reported previously, with guano-fertilised plant $\delta^{15}\text{N}$
555 experimentally enhanced by up to 20‰ relative to a control (Szpak et al., 2012),
556 a magnitude consistent with the difference between DRS sediments and local
557 plants/soils. Degradation of such N inputs to ammonia in the older MSA
558 materials is therefore a plausible source of N for the production of the alkyl
559 nitriles during pyrolysis.

560 **6.3 Leaf-wax content and distribution as burning indicators**

561 The content of extracted leaf waxes from the LSA samples (2.7 - 9.0 $\mu\text{g g}^{-1}$ dw)
562 and MSA samples (0 - 18.2 $\mu\text{g g}^{-1}$ dw; for the C_{31} *n*-alkane) are similar to
563 contemporary Lowland Fynbos soils (0.4 - 5.6 $\mu\text{g g}^{-1}$ dw; Herrmann et al., 2016).
564 The high content of leaf waxes in many SUs (Logan, Keeno, Joy, John, Ester, Eric;
565 **Fig. 7**) is in line with the input of grasses to the shelter (Cartwright, 2013; Miller
566 et al., 2013), presumably used for bedding, and supports the py-GC/MS evidence
567 for leaf cuticle input in SUs John and Jeff. The high leaf-wax content attests to
568 excellent preservation potential of these compounds within DRS, presumably
569 due either to the aridity of the shelter, or possibly to the high proportion of black
570 carbon, which may have inhibited degradation (Hernandez - Soriano et al.,
571 2016). The high content of leaf waxes also argues against extensive heating of
572 these SUs.

573 In contrast, the absence of leaf-wax *n*-alkanes in SUs Jack, Governor, Fiona, Fox,
574 Fred and Frans (**Fig. 7**) is in line with more intensive burning or heating of these
575 samples, as also inferred from the py-GC/MS: the pyrolysis products from these
576 SUs being dominated by aromatics and PAHs (**Fig. 6**). In general, SUs without *n*-

577 alkanes generally show higher proportions of PAHs, heterocyclic N and
578 aromatics in their pyrolysates, while those with high *n*-alkane abundances show
579 lower PAH, heterocyclic N and aromatics (**Fig. 10a,b**), indicating a clear relation
580 to heating.

581 Although waxes are present in SUs Leo2, Kate, Frank and Debbie, these SUs
582 exhibit lower CPIs (1.9 to 5.9) and lower ACLs (25.7 to 27.6) compared to the
583 unburnt straw and soils, which likely reflects moderate heating (**Fig. 8**). The ACL
584 values of these samples are close to those of the 300°C burning experiments of
585 Wiesenberg et al., (2009), possibly indicating heating of these samples to similar
586 temperatures (**Fig. 8**). The pyrolysates of Leo 2 and Frank are also dominated by
587 heterocyclic N products and PAHs (**Fig. 6**). Although there are differences in
588 character of the vegetation brought into DRS and the rye and maize used in the
589 laboratory burns, these temperature estimates are not inconsistent with
590 maximum temperatures measured beneath experimental fires using South
591 African vegetation (~300 °C; Sievers and Wadley, 2008). We do not observe the
592 increase in mid- and short-chain *n*-alkanes (Wiesenberg et al., 2009), although
593 this may reflect post-depositional degradation of these homologues (Cranwell,
594 1981).

595 Aside from SUs Leo2, Kate, Frank and Debbie, the remaining DRS MSA samples
596 exhibit ACL values of 28.8 to 31.0, within the range of the unburnt straw samples
597 (29.6 to 30.2) and the Succulent Karoo (30.0 ± 1.0) and Lowland Fynbos (28.8 ±
598 0.7) soils (**Fig. 8**; Carr et al., 2014), suggesting little burning. The CPI values of
599 these DRS MSA samples are in some cases lower than soils and unburnt straw
600 (**Fig. 8**), although given the high ACL values, this may reflect the sample's age

601 rather than extensive heating. We note, however, that charcoal (Miller et al.,
602 2013) and PAHs (**Fig. 6**) are present in the SUs with high ACL, suggesting that
603 these SUs represent a mixture of mainly unheated plant material and some
604 heated/burnt plant material.

605 Overall, our leaf wax data suggests that 1) some SUs (i.e. those lacking leaf
606 waxes) contain plant material that was extensively heated/burnt; 2) other SUs
607 (i.e. those with low ACL) contain plant material that was heated to 300°C or less;
608 and 3) most SUs (i.e. those with ACL similar to unburnt straw) mainly contain
609 plant material that was heated very little. Perhaps those of type 1 represent
610 direct sampling of ashes or hearths, those of type 2 represent material that was
611 positioned underneath active hearths, and type 3 represents unheated or only
612 slightly heated plant material.

613 **6.4 Organic markers compared to micromorphology**

614 Micromorphological analyses (Miller et al., 2013) identified SUs John and Jeff
615 (Lithostratigraphic Unit 3; **Fig. 10**) as containing a higher proportion of humified
616 material relative to combustion features compared with other MSA SUs. Our data
617 suggest high abundances of aliphatics, high leaf-wax content and low abundances
618 of PAHs for these SUs, in line with the micromorphological findings (**Fig. 10a,b**).

619 In contrast, SUs Governor to Debbie (Lithostratigraphic Unit 4) contain a
620 significantly higher proportion of charcoal and evidence for raking out of hearths
621 and the removal of unburnt material (Miller et al., 2013). This agrees with the
622 increased py-GC/MS indicators for black carbon (**Fig. 10a**) and decreased leaf-
623 wax content (**Fig. 10b**). Moreover, SU Fred was reported to contain burnt

624 bedding (Miller et al., 2013) and here we observe the highest PAH proportion of
625 the whole dataset and high heterocyclic N content (**Fig. 6**). Overall, our findings
626 are therefore complementary to those of the micromorphology.

627 Changes in burning and site use intensity might be expected to go hand in hand
628 with indicators of human behavioural changes, such as the abundance of
629 engraved ostrich eggshell (EOES; Texier et al., 2013). The earliest evidence for
630 EOES at DRS is between SUs Julia to Jack, which display evidence for extensive
631 burning (**Fig. 10a-c**). Similarly, going up the sequence, EOES content begins to
632 increase at SU Governor and remains high for much of Lithostratigraphic Unit 4,
633 when we observe a high degree of burning (**Fig. 10a-c**). Thus, our burning data
634 support inferences of changes in site usage and human behaviour.

635 **6.5 Vegetation-type inferences from Norm31**

636 Norm31 for the LSA (0.56 ± 0.08) is highly comparable to modern Lowland
637 Fynbos soils close to DRS (0.57 ± 0.20 ; **Fig. 9b**). Although we note the large range
638 in values of modern vegetation, this similarity would support the use of Norm31
639 as past vegetation indicator.

640 Between the Still Bay and Intermediate Howiesons Poort, Norm31 averaged 0.60
641 ± 0.05 , while during the Late Howiesons Poort it increased to 0.74 ± 0.05 (**Fig.**
642 **9b**). This Norm31 increase implies more arid-adapted vegetation was being
643 brought into the shelter during the Late Howiesons Poort. This might reflect a
644 change in the collecting habits of the inhabitants (towards more arid adapted
645 vegetation) or a change in the climate conditions/ecology around the shelter
646 towards those resembling the modern Succulent Karoo biome, such as increased

647 summer aridity. Either way, a shift in the vegetation brought into the site
648 appears to be in line with findings from charcoal remains, which suggest a shift
649 to more dry-adapted thicket vegetation during the Howiesons Poort (Cartwright,
650 2013). It should be noted that the Late, Intermediate and Early Howiesons Poort
651 were not differentiated in the charcoal study, and it is implied that the
652 aridification began during the Early Howiesons Poort. Nonetheless, the author
653 notes that the post-Howiesons Poort shows a continuing trend towards arid-
654 tolerant thicket and shrubland.

655 **6.6 $\delta^{13}\text{C}_{\text{wax}}$ and vegetation**

656 The mean $\delta^{13}\text{C}_{\text{wax}}$ for the LSA ($-29.8\text{‰} \pm 0.4\text{‰}$; **Fig. 9a**) is slightly higher than
657 soil samples from the Lowland Fynbos close to DRS ($-32.3\text{‰} \pm 2\text{‰}$; Herrmann
658 et al., 2016; **Fig. 9a**). This might reflect the selection of certain plants by the
659 inhabitants, perhaps for use as bedding or food. These values lie in between
660 those of C_3 vegetation (mean of $-34.2\text{‰} \pm 4\text{‰}$), and CAM ($-22.7\text{‰} \pm 6\text{‰}$; Boom
661 et al., 2014) and C_4 vegetation ($-21.8\text{‰} \pm 2\text{‰}$; Rommerskirchen et al, 2006),
662 thus likely reflecting input of a range of taxa using different photosynthetic
663 pathways.

664 Throughout the MSA, $\delta^{13}\text{C}_{\text{wax}}$ values exhibit little variation, varying between -
665 $29.9\text{‰} \pm 0.1\text{‰}$ and $-31.8\text{‰} \pm 0.1\text{‰}$ (**Fig. 9a**). The bulk $\delta^{13}\text{C}_{\text{TC}}$ also displays
666 limited change, of the order of 1‰ (**Fig. 4b**). Limited vegetation change is
667 implied, in line with the stability of the Fynbos biome inferred elsewhere
668 (Dupont et al., 2011). In light of the large range of values exhibited in the modern
669 soils (Herrmann et al., 2016) and plant samples (Boom et al., 2014), the small
670 variability in DRS may reflect averaging over the wide range of taxa that were

671 brought into the site through the MSA, evident in the charcoal assemblage
672 (Cartwright, 2013). Furthermore, from the $\delta^{13}\text{C}_{\text{wax}}$ stability, we can rule out
673 dominant input of the C_4 halophytic grasses into the shelter (*Spartina maritima*)
674 that today grow on the margins of the Verlorenvlei Estuary, or of CAM plants that
675 might be used as food (e.g. fruits of *Carpobrotus edulis*) or as kindling (e.g. large
676 stems of plants such as *Ruschia*).

677 **6.7 $\delta\text{D}_{\text{wax}}$ and hydroclimate**

678 The LSA mean $\delta\text{D}_{\text{wax}}$ value of $-141\text{‰} \pm 10\text{‰}$ is in line with the contemporary
679 soil samples from the DRS locale (mean of $-143\text{‰} \pm 9\text{‰}$; Herrmann et al., 2017),
680 suggesting that sedimentary $\delta\text{D}_{\text{wax}}$ is representative of the mean $\delta\text{D}_{\text{wax}}$ of
681 vegetation from the region surrounding the shelter.

682 Moreover, throughout the MSA and LSA, $\delta\text{D}_{\text{wax}}$ and $\delta^{13}\text{C}_{\text{wax}}$ values are within the
683 range of modern plants from the wider region (**Fig. 1b; 9c**). This suggests that
684 burning probably has a minor effect on $\delta\text{D}_{\text{wax}}$ and $\delta^{13}\text{C}_{\text{wax}}$. It seems that while
685 severely burnt SUs (e.g. Governor, Fred, Frans) are devoid of leaf waxes, slightly
686 heated SUs (e.g. Debbie) show comparable $\delta\text{D}_{\text{wax}}$ values to adjacent unheated SUs
687 (**Fig. 9a,c**).

688 Modern soil samples display an increase in *n*-alkane $\delta\text{D}_{\text{wax}}$ to the NE of DRS (i.e.
689 into the Succulent Karoo; **Fig. 1b**). This was interpreted (Herrmann et al., 2017)
690 to reflect: a) an increase in δD_p from SW to NE due to decreasing precipitation
691 amount, and b) a decrease in relative humidity from SW to NE, inducing
692 increased evapotranspirational isotopic enrichment of leaf and soil water. There
693 may be an additional secondary effect on $\delta\text{D}_{\text{wax}}$ associated with c) different

694 hydrogen isotope fractionation of different plant types, with C₃ trees and shrubs
695 and CAM plants tending to yield higher values than C₃ grasses (Feakins and
696 Sessions, 2010; Sachse et al., 2012).

697 Between the Still Bay and Intermediate Howiesons Poort, δD_{wax} was slightly
698 higher than the present (average $-133\text{‰} \pm 4\text{‰}$), while during the Late
699 Howiesons Poort (SUs Eve to Debbie) δD_{wax} increased further (average $-120\text{‰} \pm$
700 4‰ ; **Fig. 9c**). The Late Howiesons Poort increase likely represents input of
701 vegetation that has been subject to a) less precipitation or b) more
702 evapotranspiration (more intense summer drought), and/or may reflect c) input
703 of more shrub-like vegetation rather than grasses.

704 Input of more shrub-like vegetation during the Late Howiesons Poort would be
705 consistent with the inference of a shift to arid-adapted vegetation during the Late
706 Howiesons Poort from the Norm31 (**Fig. 9b**) and might be reflecting a shift in the
707 inhabitants' vegetation selection strategy. Such a change in inhabitants'
708 vegetation selection strategy during the Late Howiesons Poort would seem
709 plausible given the other evidence for behavioural changes including the
710 increased EOES (above Governor) and increased burning (Governor to Frans;
711 **Fig. 10**). Leaf-wax content was, however, too low for analysis between Governor
712 and Frans and so we cannot be certain that the δD_{wax} changes were coeval with
713 the site usage changes.

714 Alternatively, the δD_{wax} variability may be reflecting hydroclimate changes. The
715 above scenarios a, b and c would all broadly represent increased aridity during
716 the Late Howiesons Poort. In support of hydroclimate rather than selection
717 strategy as the control on δD_{wax} , we note that the global climate of MIS5 was

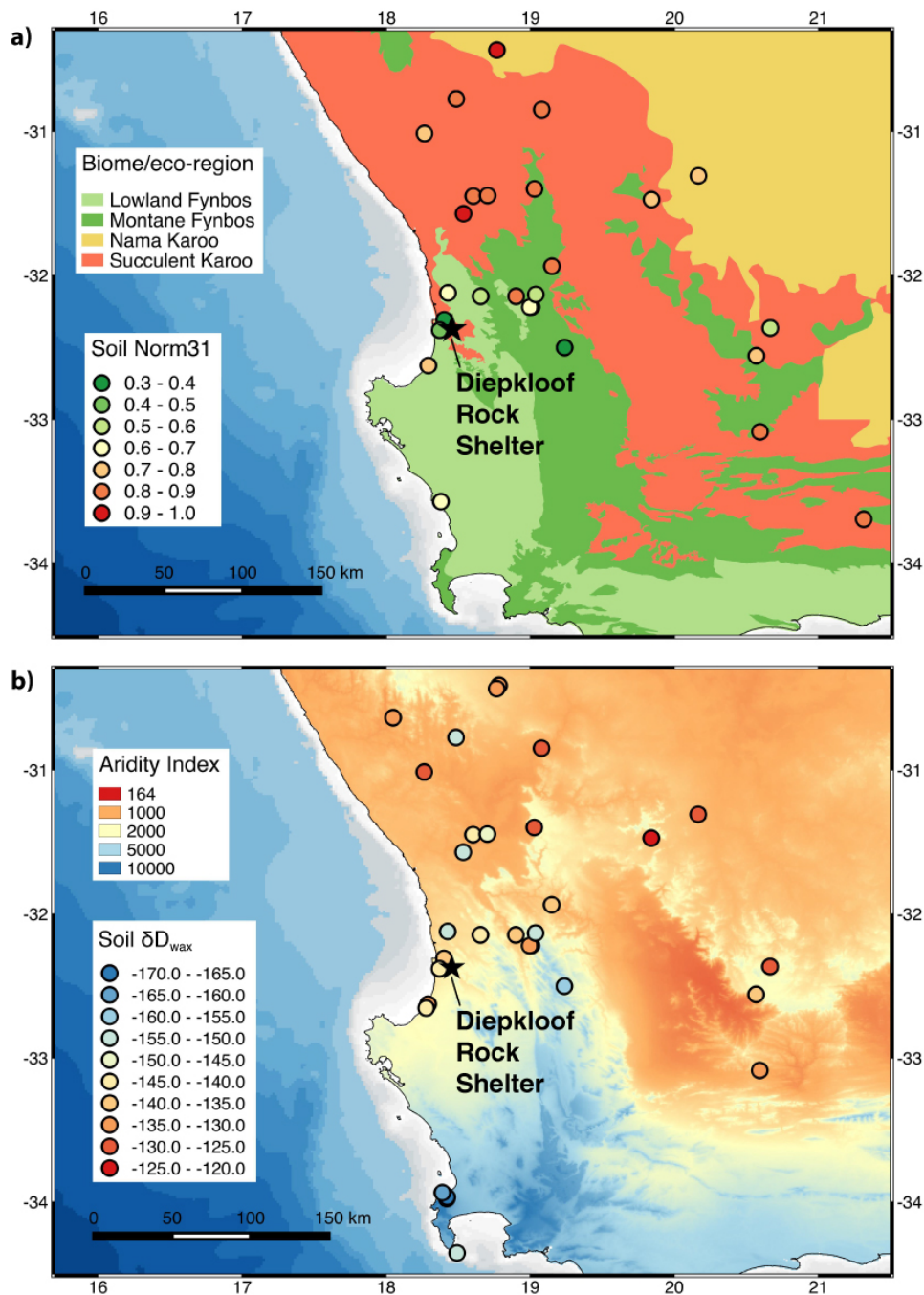
718 more similar to MIS1 than to MIS3/4, in terms of ice volume and temperature.
719 Based on the Tribolo et al., (2013) chronology, the δD_{wax} and Norm31 both
720 suggest that MIS5 (130-71ka) and MIS1 (12-0ka) were less arid, while MIS4 (71-
721 57ka) and MIS3 (57-29ka), corresponding to the Late Howiesons Poort, were
722 more arid (**Fig. 9b,c**). This might suggest that the δD_{wax} and Norm31 changes at
723 DRS were driven by aridity changes related to global climate. Nonetheless, we
724 note that this reasoning relies on a chronology that at present is controversial.

725 **7. Conclusions**

726 We investigated the potential of organic matter preserved in the MSA sediments
727 of Diepkloof Rock Shelter to understand site usage and past climate. Py-GC/MS
728 revealed that while some samples contain a high abundance of relatively un-
729 altered plant material, others were low in organic matter and are composed
730 largely of aromatic, heterocyclic N and PAH pyrolysis products, indicative of
731 higher burning intensity. The highest degree of burning is between SUs Governor
732 and Frans, in line with micromorphological findings for increased charcoal
733 content. By contrast, SUs John and Jeff display a higher abundance of humified
734 organic matter. The high N content of the sediment is interpreted as reflecting
735 inputs of hyrax urine/hyraceum and/or contributions from bird guano,
736 consistent with the high bulk $\delta^{15}N$ values.

737 We found variable but often high contents of leaf waxes. Most samples display
738 leaf-wax *n*-alkane distributions typical of modern plants in the region, suggesting
739 heating temperatures < 300°C. This is consistent with the correspondence
740 between $\delta^{13}C_{wax}$ and δD_{wax} from DRS and modern soils in the region. SUs from

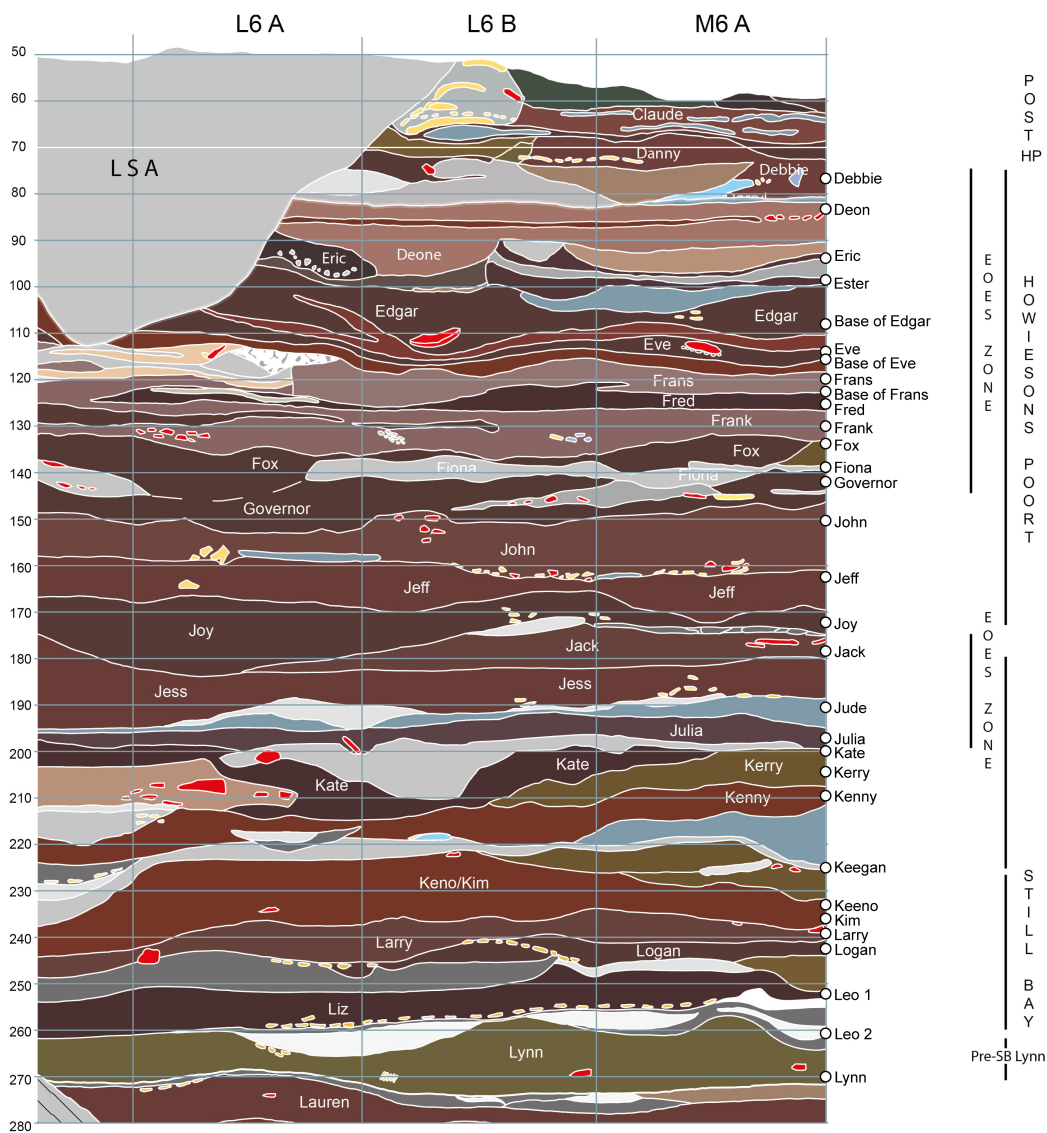
741 the Late Howiesons Poort display longer *n*-alkane chain-length distributions and
742 increased δD_{wax} values compared to the Still Bay, Intermediate Howiesons Poort
743 and the LSA. This likely represents a shift towards input of more arid-adapted
744 vegetation during the Late Howiesons Poort, reflecting aridification, or a change
745 in selection strategy of the inhabitants. Overall, these results underline the
746 potential of these organic-geochemical methods to support and augment
747 interpretations of site usage and environmental context of rock shelter
748 occupations.



750

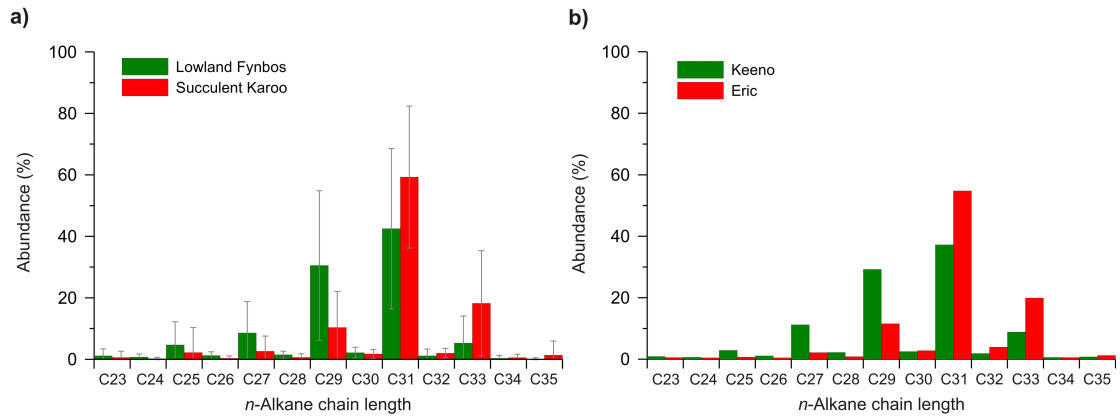
751 **Fig. 1. Maps of biomes/eco-regions and aridity. a)** Biomes and eco-regions in
 752 southwestern Africa (Rutherford et al., 2006). Circles indicate the Norm31 of *n*-
 753 alkanes from contemporary soils (Carr et al., 2014). **b)** Aridity index (Trabucco
 754 and Zomer, 2009), calculated as mean annual precipitation / mean annual
 755 potential evapotranspiration, where higher values represent less arid conditions.

756 Circles indicate the δD_{wax} (‰ VSMOW) of the C_{31} *n*-alkane from contemporary
757 soils (Herrmann et al., 2017). Bathymetry shaded grey is 0-120m depth with
758 contours every 20m.



760

761 **Fig. 2. Diepkloof Rock Shelter section.** Shown are the stratigraphic units (SUs),
 762 techno-cultural phases and the zone of high abundance of engraved ostrich
 763 eggshell (EOES). MSA samples analysed in this study were taken from square M7
 764 and are marked as white circles on the right hand edge of the figure (figure
 765 modified from Texier et al., 2013).



766

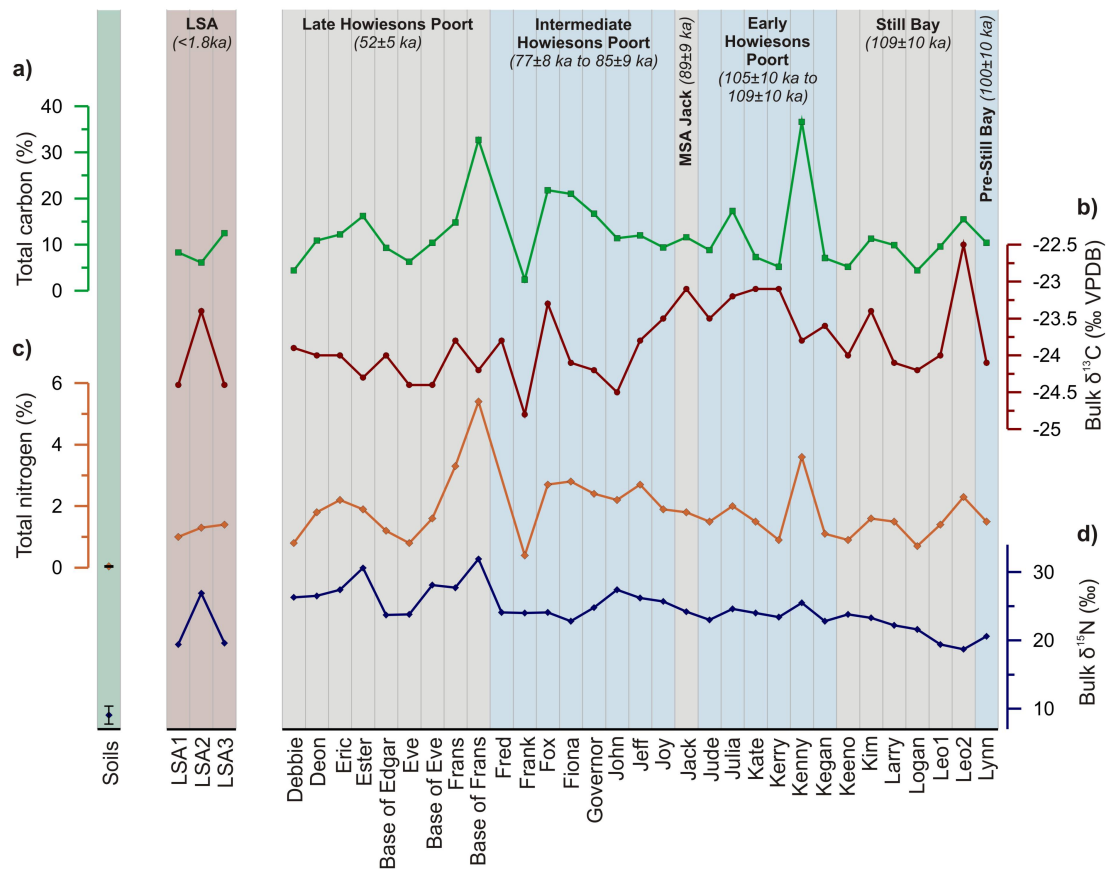
767 **Fig. 3. n-Alkane distribution in locally sourced plants and Diepkloof Rock**

768 **Shelter sediments. a)** Lowland Fynbos (n= 28) and Succulent Karoo (n=133;

769 Carr et al., 2014) plants. **b)** SU Keeno displays a Fynbos-like distribution

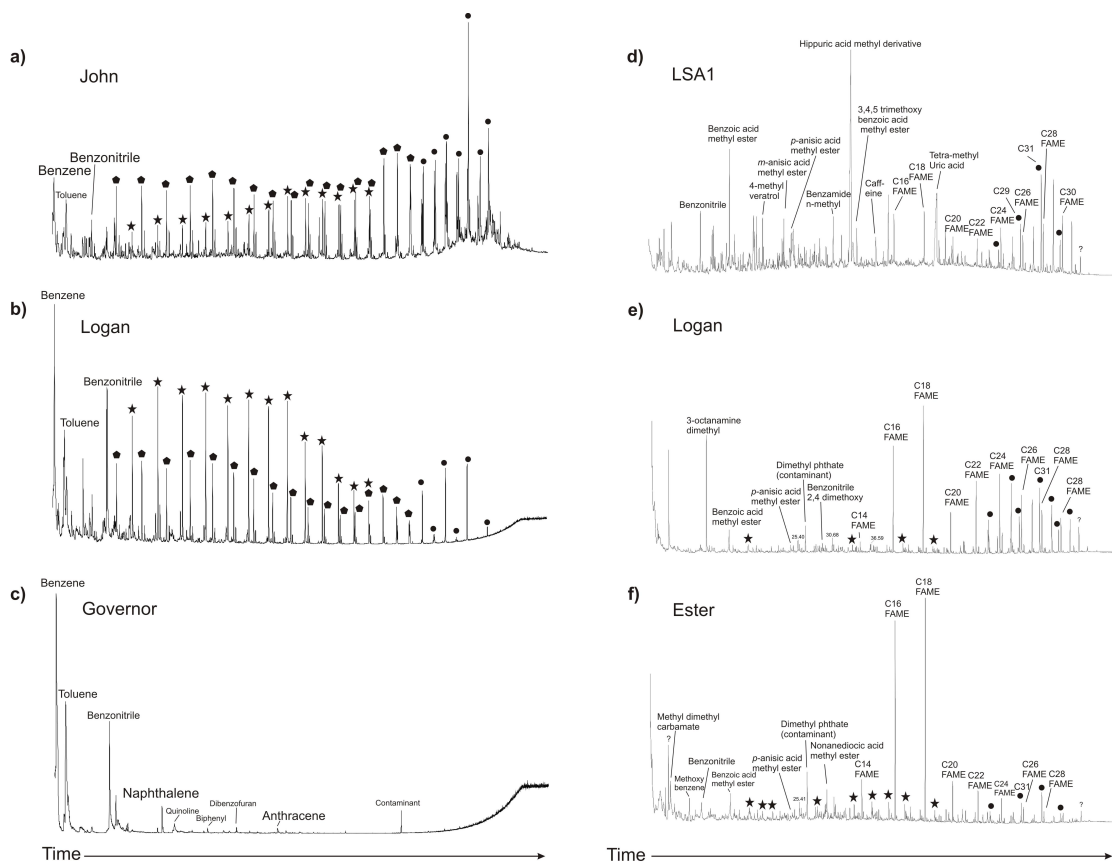
770 (dominance of C₃₁ and C₂₉), while SU Eric displays a Succulent Karoo-like

771 distribution (dominance of C₃₁ and C₃₃).



773

774 **Fig. 4. Bulk parameters for the LSA and MSA sediments. a) Total carbon**
 775 **(%TC), b) Bulk $\delta^{13}C_{TC}$ (‰ VPDB), c) Total nitrogen (%TN), d) Bulk $\delta^{15}N$ (‰).**
 776 Values of %TN and bulk $\delta^{15}N$ from modern Lowland Fynbos soils close to DRS
 777 are shown (values are mean of samples SV2-SV5 which are located within about
 778 30km of DRS; n=14; errors bars are one sigma; Carr et al. 2013 and unpublished
 779 data). Techno-cultural phases are marked above, along with the estimated ages
 780 (Tribolo et al., 2013).



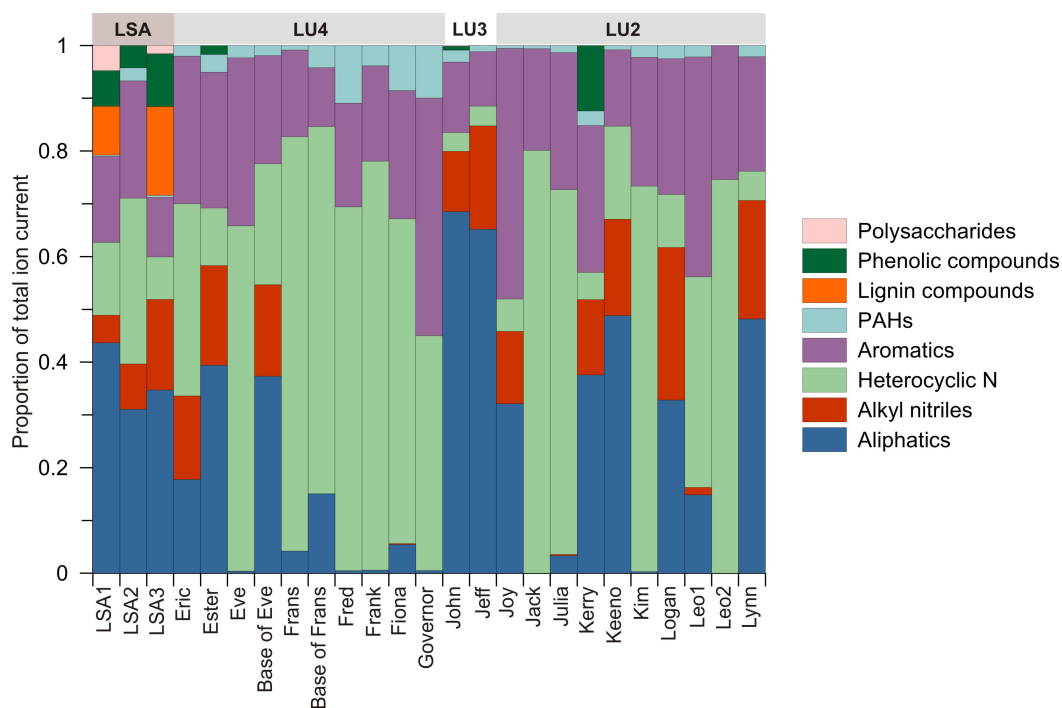
- C₂₇-C₃₃ n-alkanes with odd/even preference
- ★ Alkyl nitriles
- ◆ n-alkene/n-alkane doublets (pyrolysis products)

781

782 **Fig. 5. Pyrograms for selected samples showing the range of compounds**

783 **identified by py-GC/MS. a)-c) Selected samples run in the absence of TMAH, d)-**

784 **f) Selected samples run in the presence of TMAH.**



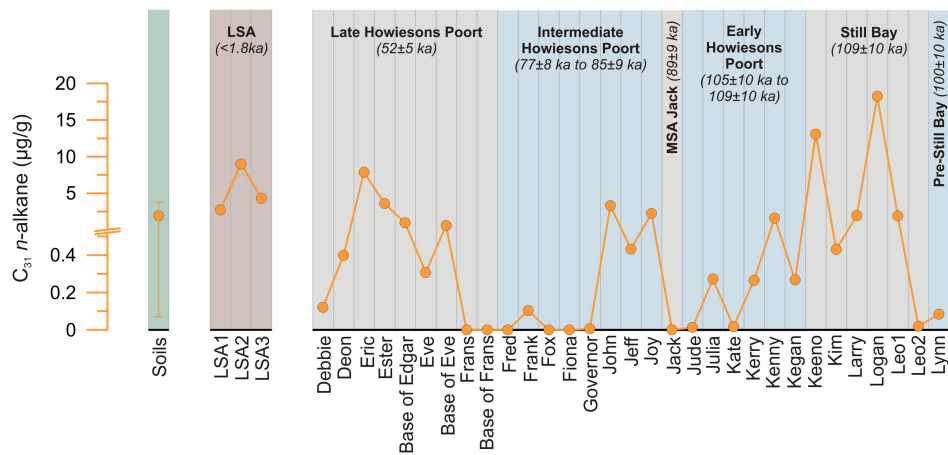
785

786 **Fig. 6. Relative proportion of compound classes in MSA and LSA sediments**

787 **derived from py-GC/MS analyses.** Shown are measurements made in the

788 absence of TMAH. Lithostratigraphic Units (LUs) as defined in Miller et al.,

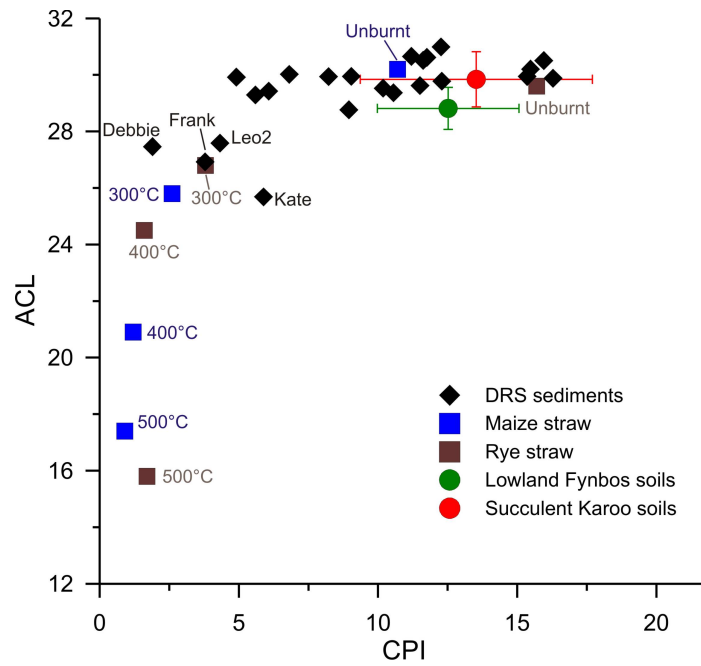
789 (2013) are given above.



790

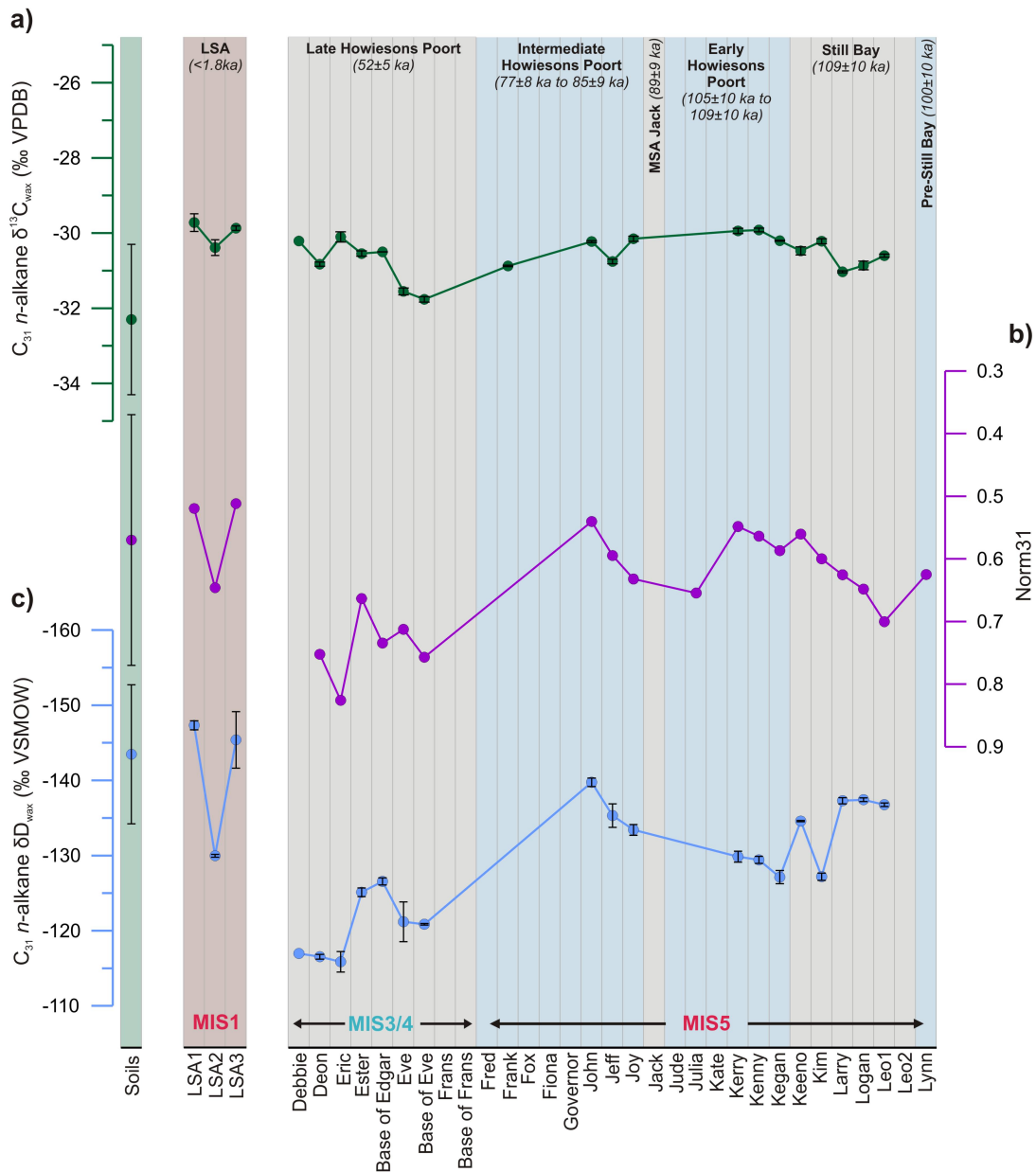
791 **Fig. 7. Leaf-wax C₃₁ n-alkane content from LSA and MSA sediments (µg g dw**
 792 **1). Techno-cultural phases are marked above (Porraz et al., 2013) along with**
 793 **their age ranges (Tribolo et al., 2013). C₃₁ n-alkane content for modern Lowland**
 794 **Fynbos soils is shown (values are mean of samples SV2-SV5, which are located**
 795 **within about 30km of DRS; n=6; error bars are one sigma; Carr et al., 2014;**
 796 **Herrmann et al., 2016).**

797



798

799 **Fig. 8. CPI₂₅₋₃₃ and ACL₁₄₋₃₅ from DRS sediments, laboratory burned straw**
800 **and soils from the region.** Black diamonds represent MSA sediments from DRS;
801 blue and brown squares represent values at different temperatures from the
802 burning experiments of maize and rye straw (Wiesenberg et al., 2009). Green
803 and red circles represent mean values from the full dataset of Lowland Fynbos
804 (n=15; error bars one sigma) and Succulent Karoo (n=53) soils (Carr et al.,
805 2014). For the straw, CPI is for C₂₇₋₃₃.



806

807 **Fig. 9. Vegetation and hydroclimate indicators from Diepkloof Rock Shelter**

808 **sediments. a)** C_{31} n-alkane $\delta^{13}C_{wax}$. Error bars represent one sigma

809 measurement precision. **b)** Norm31, (excluding samples Debbie, Frank, Kate,

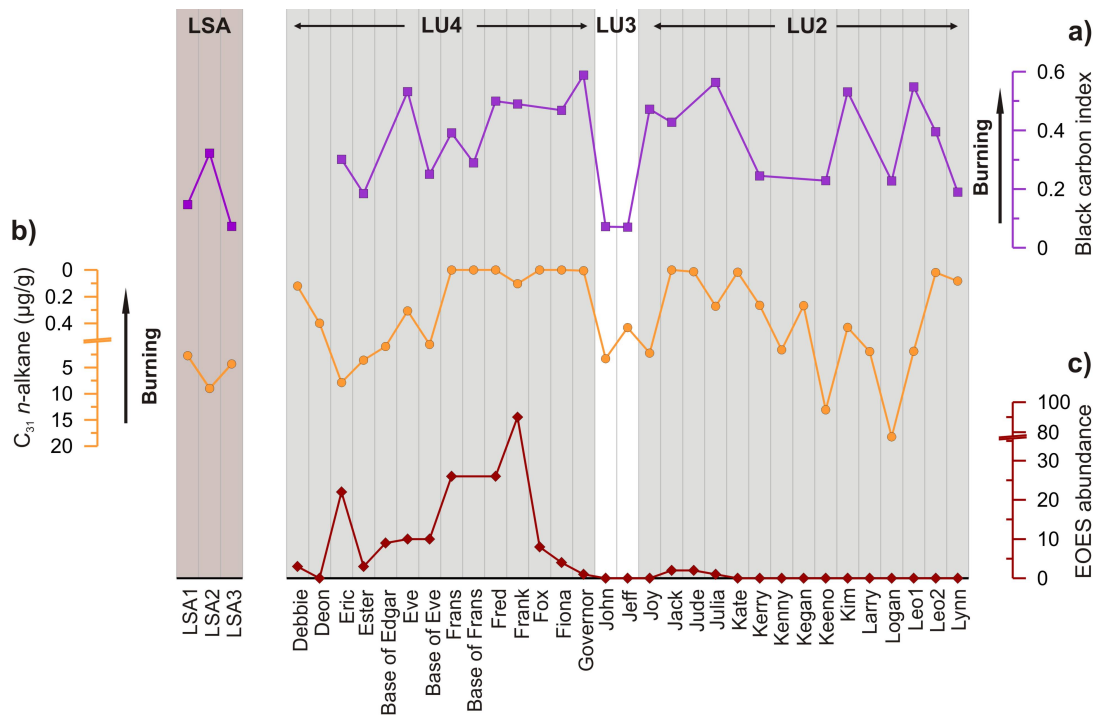
810 Leo2, which show evidence of heating). **c)** C_{31} n-alkane δD_{wax} . Error bars

811 represent one sigma measurement precision. $\delta^{13}C_{wax}$, Norm31 and δD_{wax} values

812 for modern soil samples are shown (mean of samples SV2-SV5, located within

813 about 30km of DRS; n=6; error bars are one sigma; Herrmann et al., 2016, 2017).

814 Marine Isotope Stages (MIS) into which the SUs fall (based on the age model of
815 Tribolo et al., 2013) are marked.



816

817 **Fig. 10. Summary of burning indicators and EOES. a)** Black carbon index,
 818 which is the sum of the relative proportion of benzene, toluene, naphthalene,
 819 biphenyl, dibenzofuran and benzonitrile (Kaal and Rumpel, 2009). **b)** C_{31} *n*-
 820 alkane content (note inverted axis), **c)** Number of engraved ostrich eggshells
 821 (EOES) within each SU (Texier et al., 2013). Lithostratigraphic Units (LUs) 2-4
 822 are marked (Miller et al., 2013).

823 **Acknowledgements**

824 Excavations at Diepkloof were funded by the French Ministry of Foreign Affairs
825 (MAE), the Aquitaine region, the Provence-Alpes-Côte-d'Azur region, the Centre
826 National de la Recherche Scientifique (CNRS) as well as by the Palaeontological
827 Scientific Trust (PAST) and the National Research Foundation (NRF) of South
828 Africa. D. & M. van Wyk and J. Pollet gave permission for the excavations to take
829 place. We thank Guillaume Porraz and Pierre-Jean Texier for allowing us to take
830 sediment samples, and facilitating this process in the field. Christopher Miller
831 provided invaluable help during sampling. Ian Newton, Nicoletta Ruggieri and
832 Ralph Kreutz are thanked for their assistance in the lab. Thanks to Pierre-Jean
833 Texier for providing the stratigraphic section in Figure 2, and Matthew Lewis for
834 assistance with modifying it. Emma Pearson is thanked for providing additional
835 soil samples from South Africa. Data from those samples have been generated by
836 Katharina Siedenbergh. James A. Collins was funded by the Helmholtz Postdoc
837 Programme (PD-001) and the Alfred Wegener Institute for Polar and Marine
838 Research, Bremerhaven. Judith Sealy acknowledges support from the South
839 African Research Chairs initiative of the Department of Science and Technology
840 and National Research Foundation of South Africa. The compound-specific
841 isotope analyses were supported by the DFG-Research Center / Cluster of
842 Excellence „The Ocean in the Earth System“ at MARUM - Center for Marine
843 Environmental Sciences.

844 **Conflicts of interest**

845 The authors declare that they have no conflict of interest.

846 **References**

- 847 Ballentine, D.C., Macko, S.A., Turekian, V.C., 1998. Variability of stable
848 carbon isotopic compositions in individual fatty acids from combustion of C₄ and
849 C₃ plants: implications for biomass burning. *Chem. Geol.* 152, 151-161.
- 850 Bird, M.I., Tait, E., Wurster, C.M., Furness, R.W., 2008. Stable carbon and
851 nitrogen isotope analysis of avian uric acid. *Rapid Commun. Mass Spectrom.* 22,
852 3393-3400.
- 853 Boom, A., Carr, A., Chase, B., Grimes, H., Meadows, M., 2014. Leaf wax n-
854 alkanes and $\delta^{13}\text{C}$ values of CAM plants from arid southwest Africa. *Org.*
855 *Geochem.* 67, 99-102.
- 856 Braadbaart, F., Boon, J.J., Veld, H., David, P., van Bergen, P.F., 2004.
857 Laboratory simulations of the transformation of peas as a result of heat
858 treatment: changes of the physical and chemical properties. *Journal of*
859 *Archaeological Science* 31, 821-833.
- 860 Braadbaart, F., Poole, I., 2008. Morphological, chemical and physical
861 changes during charcoalification of wood and its relevance to archaeological
862 contexts. *Journal of archaeological science* 35, 2434-2445.
- 863 Carr, A.S., Boom, A., Chase, B.M., 2010a. The potential of plant biomarker
864 evidence derived from rock hyrax middens as an indicator of
865 palaeoenvironmental change. *Palaeogeogr. Palaeoclimatol. Palaeoecol.* 285, 321-
866 330.
- 867 Carr, A.S., Boom, A., Chase, B.M., Meadows, M.E., Roberts, Z.E., Britton,
868 M.N., Cumming, A.M., 2013. Biome-scale characterisation and differentiation of

869 semi-arid and arid zone soil organic matter compositions using pyrolysis–GC/MS
870 analysis. *Geoderma* 200, 189-201.

871 Carr, A.S., Boom, A., Chase, B.M., Roberts, D.L., Roberts, Z.E., 2010b.
872 Molecular fingerprinting of wetland organic matter using pyrolysis-GC/MS: an
873 example from the southern Cape coastline of South Africa. *J. Paleolimnol.* 44,
874 947-961.

875 Carr, A.S., Boom, A., Grimes, H.L., Chase, B.M., Meadows, M.E., Harris, A.,
876 2014. Leaf wax n-alkane distributions in arid zone South African flora:
877 environmental controls, chemotaxonomy and palaeoecological implications. *Org.*
878 *Geochem.* 67, 72-84.

879 Carr, A.S., Chase, B.M., Boom, A., Medina-Sanchez, J., 2016a. Stable isotope
880 analyses of rock hyrax faecal pellets, hyraceum and associated vegetation in
881 southern Africa: Implications for dietary ecology and palaeoenvironmental
882 reconstructions. *Journal of Arid Environments* 134, 33-48.

883 Carr, A.S., Chase, B.M., Mackay, A., 2016b. Mid to Late Quaternary
884 landscape and environmental dynamics in the Middle Stone Age of southern
885 South Africa, Africa from MIS 6-2. Springer, pp. 23-47.

886 Cartwright, C.R., 2013. Identifying the woody resources of Diepkloof Rock
887 Shelter (South Africa) using scanning electron microscopy of the MSA wood
888 charcoal assemblages. *Journal of Archaeological Science* 40, 3463-3474.

889 Challinor, J.M., 2001. Review: the development and applications of
890 thermally assisted hydrolysis and methylation reactions. *J. Anal. Appl. Pyrolysis*
891 61, 3-34.

892 Charrié-Duhaut, A., Porraz, G., Cartwright, C.R., Igreja, M., Connan, J.,
893 Poggenpoel, C., Texier, P.-J., 2013. First molecular identification of a hafting

894 adhesive in the late Howiesons Poort at Diepkloof Rock Shelter (Western Cape,
895 South Africa). *Journal of Archaeological Science* 40, 3506-3518.

896 Chase, B.M., 2010. South African palaeoenvironments during marine
897 oxygen isotope stage 4: a context for the Howiesons Poort and Still Bay
898 industries. *Journal of Archaeological Science* 37, 1359-1366.

899 Cowling, R.M., Richardson, D.M., Mustart, P.J., 1997. Fynbos, in: Cowling,
900 R.W., Richardson, D.M., Pierce, S.M. (Eds.), *Vegetation of Southern Africa*.
901 Cambridge University Press, Cambridge, pp. 99–130.

902 Cranwell, P., 1981. Diagenesis of free and bound lipids in terrestrial
903 detritus deposited in a lacustrine sediment. *Org. Geochem.* 3, 79-89.

904 Dayet, L., Texier, P.-J., Daniel, F., Porraz, G., 2013. Ochre resources from
905 the Middle Stone Age sequence of Diepkloof Rock Shelter, Western Cape, South
906 Africa. *Journal of Archaeological Science* 40, 3492-3505.

907 Del Rio, J.C., Hatcher, P.G., 1998. Analysis of aliphatic biopolymers using
908 thermochemolysis with tetramethylammonium hydroxide (TMAH) and gas
909 chromatography-mass spectrometry. *Org. Geochem.* 29, 1441-1451.

910 Dupont, L.M., Linder, H.P., Rommerskirchen, F., Schefuß, E., 2011.
911 Climate - driven rampant speciation of the Cape flora. *Journal of Biogeography*
912 38, 1059-1068.

913 Eckmeier, E., Wiesenberg, G.L., 2009. Short-chain n-alkanes (C16–20) in
914 ancient soil are useful molecular markers for prehistoric biomass burning.
915 *Journal of Archaeological Science* 36, 1590-1596.

916 Eglinton, G., Hamilton, R.J., 1967. Leaf Epicuticular Waxes. *Science* 156,
917 1322-1335.

918 Eglinton, T.I., Eglinton, G., 2008. Molecular proxies for paleoclimatology.
919 Earth Planet. Sci. Lett. 275, 1-16.

920 Feakins, S.J., Sessions, A.L., 2010. Controls on the D/H ratios of plant leaf
921 waxes in an arid ecosystem. *Geochim. Cosmochim. Acta* 74, 2128-2141.

922 Feathers, J., 2015. Luminescence dating at Diepkloof Rock Shelter–new
923 dates from single-grain quartz. *Journal of Archaeological Science* 63, 164-174.

924 Fezzy, S., Armitage, R.A., 2006. Pyrolysis GC–MS and THM-GC–MS studies
925 of a black coating from Little Lost River Cave, Idaho. *J. Anal. Appl. Pyrolysis* 77,
926 102-110.

927 Goldberg, P., Miller, C.E., Schiegl, S., Ligouis, B., Berna, F., Conard, N.J.,
928 Wadley, L., 2009. Bedding, hearths, and site maintenance in the Middle Stone age
929 of Sibudu cave, KwaZulu-Natal, South Africa. *Archaeological and Anthropological*
930 *Sciences* 1, 95-122.

931 Goñi, M.A., Hedges, J.I., 1992. Lignin dimers: Structures, distribution, and
932 potential geochemical applications. *Geochim. Cosmochim. Acta* 56, 4025-4043.

933 Henshilwood, C.S., d'Errico, F., Yates, R., Jacobs, Z., Tribolo, C., Duller, G.A.,
934 Mercier, N., Sealy, J.C., Valladas, H., Watts, I., 2002. Emergence of modern human
935 behavior: Middle Stone Age engravings from South Africa. *Science* 295, 1278-
936 1280.

937 Hernandez - Soriano, M.C., Kerré, B., Goos, P., Hardy, B., Dufey, J.,
938 Smolders, E., 2016. Long - term effect of biochar on the stabilization of recent
939 carbon: soils with historical inputs of charcoal. *GCB Bioenergy* 8, 371-381.

940 Herrmann, N., Boom, A., Carr, A.S., Chase, B.M., Granger, R., Hahn, A., Zabel,
941 M., Schefuß, E., 2016. Sources, transport and deposition of terrestrial organic
942 material: A case study from southwestern Africa. *Quat. Sci. Rev.* 149, 215-229.

943 Herrmann, N., Boom, A., Carr, A.S., Chase, B.M., West, A.G., Zabel, M.,
944 Schefuß, E., 2017. Hydrogen isotope fractionation of leaf wax n-alkanes in
945 southern African soils. *Org. Geochem.* 109, 1-13.

946 Hijmans, R.J., Cameron, S.E., Parra, J.L., Jones, P.G., Jarvis, A., 2005. Very
947 high resolution interpolated climate surfaces for global land areas. *International*
948 *journal of climatology* 25, 1965-1978.

949 Jacobs, Z., Roberts, R.G., 2015. An improved single grain OSL chronology
950 for the sedimentary deposits from Diepkloof Rockshelter, Western Cape, South
951 Africa. *Journal of Archaeological Science* 63, 175-192.

952 Jacobs, Z., Roberts, R.G., Galbraith, R.F., Deacon, H.J., Grün, R., Mackay, A.,
953 Mitchell, P., Vogelsang, R., Wadley, L., 2008. Ages for the Middle Stone Age of
954 southern Africa: implications for human behavior and dispersal. *Science* 322,
955 733-735.

956 Kaal, J., Baldock, J.A., Buurman, P., Nierop, K.G., Pontevedra-Pombal, X.,
957 Martínez-Cortizas, A., 2007. Evaluating pyrolysis-GC/MS and ¹³C CPMAS NMR in
958 conjunction with a molecular mixing model of the Penido Vello peat deposit, NW
959 Spain. *Org. Geochem.* 38, 1097-1111.

960 Kaal, J., Cortizas, A.M., Nierop, K.G., 2009. Characterisation of aged
961 charcoal using a coil probe pyrolysis-GC/MS method optimised for black carbon.
962 *J. Anal. Appl. Pyrolysis* 85, 408-416.

963 Kaal, J., Rumpel, C., 2009. Can pyrolysis-GC/MS be used to estimate the
964 degree of thermal alteration of black carbon? *Org. Geochem.* 40, 1179-1187.

965 Kaal, J., Schneider, M.P., Schmidt, M.W., 2012. Rapid molecular screening
966 of black carbon (biochar) thermosequences obtained from chestnut wood and
967 rice straw: A pyrolysis-GC/MS study. *Biomass Bioenergy* 45, 115-129.

968 Mallol, C., Hernández, C.M., Cabanes, D., Sistiaga, A., Machado, J.,
969 Rodríguez, Á., Pérez, L., Galván, B., 2013. The black layer of Middle Palaeolithic
970 combustion structures. Interpretation and archaeostratigraphic implications.
971 *Journal of Archaeological Science* 40, 2515-2537.

972 Masiello, C.A., 2004. New directions in black carbon organic geochemistry.
973 *Mar. Chem.* 92, 201-213.

974 Miller, C.E., Goldberg, P., Berna, F., 2013. Geoarchaeological investigations
975 at Diepkloof Rock Shelter, Western Cape, South Africa. *Journal of Archaeological*
976 *Science* 40, 3432-3452.

977 Milton, S.J., Yeaton, R.I., Dean, W.R.J., Vlok, J.H.J., 1997. Succulent Karoo, in:
978 Cowling, R.W., Richardson, D.M., Pierce, S.M. (Eds.), *Vegetation of Southern*
979 *Africa*. Cambridge University Press, Cambridge, pp. 131–166.

980 Mizutani, H., Wada, E., 1985. High-performance liquid chromatographic
981 determination of uric acid in soil. *J. Chromatogr. A* 331, 359-369.

982 Nierop, K.G., van Bergen, P.F., 2002. Clay and ammonium catalyzed
983 reactions of alkanols, alkanolic acids and esters under flash pyrolytic conditions.
984 *J. Anal. Appl. Pyrolysis* 63, 197-208.

985 Parkington, J., Poggenpoel, C., 1987. Diepkloof rock shelter, *Papers in the*
986 *prehistory of the western Cape, South Africa*. Oxford: BAR International Series,
987 pp. 269-293.

988 Poole, I., Braadbaart, F., Boon, J.J., van Bergen, P.F., 2002. Stable carbon
989 isotope changes during artificial charring of propagules. *Org. Geochem.* 33, 1675-
990 1681.

991 Porraz, G., Texier, P.-J., Archer, W., Piboule, M., Rigaud, J.-P., Tribolo, C.,
992 2013. Technological successions in the Middle Stone Age sequence of Diepkloof

993 Rock Shelter, Western Cape, South Africa. *Journal of Archaeological Science* 40,
994 3376-3400.

995 Poynter, J., Farrimond, P., Robinson, N., Eglinton, G., 1989. Aeolian-derived
996 higher plant lipids in the marine sedimentary record: Links with palaeoclimate,
997 Paleoclimatology and paleometeorology: modern and past patterns of global
998 atmospheric transport. Springer, pp. 435-462.

999 Rommerskirchen, F., Plader, A., Eglinton, G., Chikaraishi, Y., Rullkötter, J.,
1000 2006. Chemotaxonomic significance of distribution and stable carbon isotopic
1001 composition of long-chain alkanes and alkan-1-ols in C4 grass waxes. *Org.*
1002 *Geochem.* 37, 1303-1332.

1003 Rozanski, K., Araguás-Araguás, L., Gonfiantini, R., 1993. Isotopic patterns
1004 in modern global precipitation. In: Savin, S. (Eds.). *Climate Change in Continental*
1005 *Isotopic Records*. American Geophysical Union, Washington, DC, pp. 1-36.

1006 Rundel, P.W., Esler, K.J., Cowling, R.M., 1999. Ecological and phylogenetic
1007 patterns of carbon isotope discrimination in the winter-rainfall flora of the
1008 Richtersveld, South Africa. *Plant Ecology* 142, 133-148.

1009 Rutherford, M.C., Mucina, L., Powrie, L.W., 2006. Biomes and Bioregions of
1010 Southern Africa. , in: Mucina, L., Rutherford, M.C. (Eds.), *The vegetation of South*
1011 *Africa, Lesotho and Swaziland*. South African National Biodiversity Institute,
1012 Pretoria, pp. 30-51.

1013 Sachse, D., Billault, I., Bowen, G.J., Chikaraishi, Y., Dawson, T.E., Feakins,
1014 S.J., Freeman, K.H., Magill, C.R., McInerney, F.A., van der Meer, M.T.J., Polissar, P.,
1015 Robins, R.J., Sachs, J.P., Schmidt, H.-L., Sessions, A.L., White, J.W.C., West, J.B.,
1016 Kahmen, A., 2012. *Molecular Paleohydrology: Interpreting the Hydrogen-Isotopic*

1017 Composition of Lipid Biomarkers from Photosynthesizing Organisms. Annual
1018 Review of Earth and Planetary Sciences 40, 221-249.

1019 Sáiz-Jiménez, C., 1994. Analytical pyrolysis of humic substances: pitfalls,
1020 limitations, and possible solutions. Environmental science & technology 28,
1021 1773-1780.

1022 Sáiz-Jiménez, C., De Leeuw, J., 1986. Chemical characterization of soil
1023 organic matter fractions by analytical pyrolysis-gas chromatography-mass
1024 spectrometry. J. Anal. Appl. Pyrolysis 9, 99-119.

1025 Schefuß, E., Ratmeyer, V., Stuut, J.-B.W., Jansen, J.H.F., Sinninghe Damsté,
1026 J.S., 2003. Carbon isotope analyses of *n*-alkanes in dust from the lower
1027 atmosphere over the central eastern Atlantic. Geochim. Cosmochim. Acta 67,
1028 1757-1767.

1029 Sealy, J.C., Van Der Merwe, N.J., Thorp, J.A.L., Lanham, J.L., 1987. Nitrogen
1030 isotopic ecology in southern Africa: implications for environmental and dietary
1031 tracing. Geochim. Cosmochim. Acta 51, 2707-2717.

1032 Simoneit, B.R., 2002. Biomass burning—a review of organic tracers for
1033 smoke from incomplete combustion. Appl. Geochem. 17, 129-162.

1034 Steele, T.E., Klein, R.G., 2013. The Middle and Later Stone Age faunal
1035 remains from Diepkloof Rock Shelter, Western Cape, South Africa. Journal of
1036 Archaeological Science 40, 3453-3462.

1037 Stock, W., Wienand, K., Baker, A., 1995. Impacts of invading N₂-fixing
1038 Acacia species on patterns of nutrient cycling in two Cape ecosystems: evidence
1039 from soil incubation studies and ¹⁵N natural abundance values. Oecologia 101,
1040 375-382.

1041 Szpak, P., Millaire, J.-F., White, C.D., Longstaffe, F.J., 2012. Influence of
1042 seabird guano and camelid dung fertilization on the nitrogen isotopic
1043 composition of field-grown maize (*Zea mays*). *Journal of Archaeological Science*
1044 39, 3721-3740.

1045 Texier, P.-J., Porraz, G., Parkington, J., Rigaud, J.-P., Poggenpoel, C., Miller,
1046 C., Tribolo, C., Cartwright, C., Coudenneau, A., Klein, R., 2010. A Howiesons Poort
1047 tradition of engraving ostrich eggshell containers dated to 60,000 years ago at
1048 Diepkloof Rock Shelter, South Africa. *Proceedings of the National Academy of*
1049 *Sciences* 107, 6180-6185.

1050 Texier, P.-J., Porraz, G., Parkington, J., Rigaud, J.-P., Poggenpoel, C., Tribolo,
1051 C., 2013. The context, form and significance of the MSA engraved ostrich eggshell
1052 collection from Diepkloof Rock Shelter, Western Cape, South Africa. *Journal of*
1053 *Archaeological Science* 40, 3412-3431.

1054 Thevenot, M., Dignac, M.-F., Rumpel, C., 2010. Fate of lignins in soils: a
1055 review. *Soil Biol. Biochem.* 42, 1200-1211.

1056 Trabucco, A., Zomer, R.J., 2009. Global Potential Evapo-Transpiration
1057 (Global-PET) and Global Aridity Index (Global-Aridity) Geo-Database. CGIAR
1058 Consortium for Spatial Information. Available online from the CGIAR-CSI
1059 GeoPortal at: <http://www.csi.cgiar.org>.

1060 Tribolo, C., Mercier, N., Douville, E., Joron, J.-L., Reyss, J.-L., Rufer, D.,
1061 Cantin, N., Lefrais, Y., Miller, C., Porraz, G., 2013. OSL and TL dating of the Middle
1062 Stone Age sequence at Diepkloof Rock Shelter (South Africa): a clarification.
1063 *Journal of Archaeological Science* 40, 3401-3411.

1064 Tribolo, C., Mercier, N., Valladas, H., Joron, J.-L., Guibert, P., Lefrais, Y., Selo,
1065 M., Texier, P.-J., Rigaud, J.-P., Porraz, G., 2009. Thermoluminescence dating of a

1066 Stillbay–Howiesons Poort sequence at Diepkloof Rock Shelter (Western Cape,
1067 South Africa). *Journal of Archaeological Science* 36, 730-739.

1068 Vancampenhout, K., Wouters, K., Caus, A., Buurman, P., Swennen, R.,
1069 Deckers, J., 2008. Fingerprinting of soil organic matter as a proxy for assessing
1070 climate and vegetation changes in last interglacial palaeosols (Veldwezelt,
1071 Belgium). *Quaternary Research* 69, 145-162.

1072 Vogel, J.C., Fuls, A., Ellis, R.P., 1978. Geographical distribution of Kranz
1073 grasses in South Africa. *S. Afr. J. Sci.*

1074 Vogts, A., Moossen, H., Rommerskirchen, F., Rullkötter, J., 2009.
1075 Distribution patterns and stable carbon isotopic composition of alkanes and
1076 alkan-1-ols from plant waxes of African rain forest and savanna C₃ species. *Org.*
1077 *Geochem.* 40, 1037-1054.

1078 Wadley, L., 2015. Those marvellous millennia: the Middle Stone Age of
1079 Southern Africa. *Azania: Archaeological Research in Africa* 50, 155-226.

1080 Wadley, L., Sievers, C., Bamford, M., Goldberg, P., Berna, F., Miller, C., 2011.
1081 Middle Stone Age bedding construction and settlement patterns at Sibudu, South
1082 Africa. *Science* 334, 1388-1391.

1083 Wiesenberg, G., Lehndorff, E., Schwark, L., 2009. Thermal degradation of
1084 rye and maize straw: lipid pattern changes as a function of temperature. *Org.*
1085 *Geochem.* 40, 167-174.

1086
1087
1088
1089
1090